He Huang, Hendrik du Toit, Luca Panariello, Luca Mazzei
and Asterios Gavriilidis

4 Continuous synthesis of gold nanoparticles in micro- and millifluidic systems

Abstract: Gold nanomaterials have diverse applications ranging from healthcare and nanomedicine to analytical sciences and catalysis. Microfluidic and millifluidic reactors offer multiple advantages for their synthesis and manufacturing, including controlled or fast mixing, accurate reaction time control and excellent heat transfer. These advantages are demonstrated by reviewing gold nanoparticle synthesis strategies in flow devices. However, there are still challenges to be resolved, such as reactor fouling, particularly if robust manufacturing processes are to be developed to achieve the desired targets in terms of nanoparticle size, size distribution, surface properties, process throughput and robustness. Solutions to these challenges are more effective through a coordinated approach from chemists, engineers and physicists, which has at its core a qualitative and quantitative understanding of the synthesis processes and reactor operation. This is important as nanoparticle synthesis is complex, encompassing multiple phenomena interacting with each other, often taking place at short timescales. The proposed methodology for the development of reactors and processes is generic and contains various interconnected considerations. It aims to be a starting point towards rigorous design procedures for the robust and reproducible continuous flow synthesis of gold nanoparticles.

This article has previously been published in the journal *Physical Sciences Reviews*. Please cite as: Huang, H., du Toit, H., Panariello, L., Mazzei, L., Gavriilidis, A. Continuous synthesis of gold nanoparticles in micro- and millifluidic systems. *Physical Sciences Reviews* [Online] **2018**, 3. DOI: 10.1515/psr-2017-0119

https://doi.org/10.1515/9783110345100-004

Graphical Abstract:

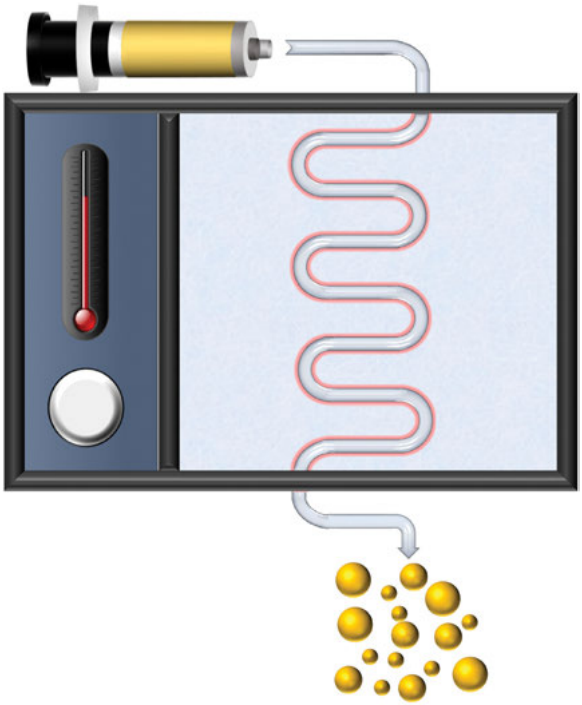

Keywords: gold nanomaterials, flow chemistry, microfluidics, microreactors, milli-reactors, multiphase flow

4.1 Introduction

4.1.1 Applications of gold nanoparticles

Gold nanomaterials have been a topic of intense investigation in the last few decades owing to their unique optical, chemical, biological and catalytic properties. This is due to some attractive physical characteristics, which are determined by physical parameters such as particle size, morphology, surface, crystallinity and composition. Gold nanomaterials are attracting a lot of interest in healthcare applications, analytical sciences and catalysis [1–7]. In nanomedicine, Au nanomaterials offer the potential to work on the same scale as many biological processes and cellular mechanisms. They are applied as diagnostic, imaging and therapeutic agents or a combination thereof [4, 5].

When Au nanoparticles (NPs) are illuminated, conduction band electrons on their surface are delocalized and undergo collective oscillation at the same frequency as the incident light. This phenomenon, known as localized surface plasmon resonance (LSPR), is responsible for absorption and scattering of light, which can aid their detection by optical microscopy and enhance optical contrast as well as lead to localized heating [8, 9]. The LSPR effect is sensitive to the size, shape and environment of the NPs and this allows tuning their optical properties. If analyte molecules bind to Au NPs either directly or via some linker ligands, the local refractive index changes and the plasmon absorption shifts to longer wavelengths. The former results in colour change, which makes NPs attractive for colorimetric sensors, while the latter can be detected both by LSPR extinction or the angle of reflected light and are exploited in other plasmonic sensors [5, 10]. Electric fields generated on the surface of the NPs enhance Raman signals from molecules in their vicinity. This is termed as surface enhanced Raman scattering [11]. Light absorption by very small NPs (nanoclusters) induces photoluminescence, which is affected if analyte molecules interact with the nanoclusters, either through covalent bonding or physical absorption. Fluorescence quenching is another phenomenon that occurs when fluorophores are appended onto Au NPs, and this is exploited in fluorescence resonance energy transfer assays [6, 12].

In addition to the above optical properties, Au NPs demonstrate catalytic properties, which can be tuned by particle size, surface functionality and intraparticle separation. Such properties are exploited in various electrochemical and electrocatalytic sensors. These optical, optoelectronic, electrochemical and electrocatalytic properties are utilized for detection of biomolecules, such as proteins, DNA, oligonucleotides and pathogens, but also whole cancer cells which are important for healthcare applications [6, 7, 11, 13–15]. In addition, the same properties can be applied for sensing various chemical compounds, such as heavy metal ions, toxic gases and organic compounds, which are important for environmental and safety applications [12, 16]. In Lateral Flow Assays, Au nanomaterials are conjugated with various recognition markers, such as antibodies, and implemented in paper-based devices. They offer low-cost, robust, point of care diagnostics for the detection of viruses, bacteria, biomarkers, proteins, drugs, hormones contaminants, toxins and pathogens [10, 17–21]. By conjugating the NPs to molecules that bind to cells, the above optical properties can be exploited for cellular imaging (e. g. stem cells and cancer cells). The NPs can also be used for enhancing contrast of other imaging modalities. Au NPs can enhance X-ray attenuation increasing contrast in X-ray CT imaging [6]. Au nanostructures can be functionalized by radionucleotides and hence used for PET imaging of tumours [6, 7].

In targeted drug delivery, a drug is delivered locally to the tissue of interest, leaving surrounding tissues unaffected. The drug concentration can be modulated as a function of time. This approach offers various advantages, such as decreased toxic side effects, reduced dose of drugs, increased treating efficacy and development of new therapeutic strategies extending product life cycles [22]. Drug molecules can be

loaded onto the surface of Au nanostructures by direct conjugation, grafting the drugs to the capping ligand or adsorbing the drug by electrostatic interactions, van der Waals forces or hydrogen bonding. Targeting agents can be attached to Au NPs for specific uptake by tumours. The release of the drug can be achieved by thermally activated desorption and diffusion employing the selective heating ability of the Au nanostructures. To increase the amount of drug, the drug can by encapsulated in thermally responsive polymers. The stimulus for drug release can also be a change in ionic concentration [6, 7, 23].

Au nanomaterials (mainly Au nanorods, nanoshells and nanocages) have been studied for photothermal cancer therapy, which is based on their LSPR properties. They absorb and convert the photon energy into thermal energy when a laser beam irradiates them at the LSPR wavelength. Photothermal heating only occurs in the area directly surrounding the NPs, damaging cancer cells, particularly those that are more sensitive to heat. By exploiting the enhanced permeability and retention of tumours (passive targeting), or by functionalizing NPs with molecules that selectively bind to cancer cells (active targeting), NPs deliver the heat selectively to tumour sites [6, 7, 23–26]. In photodynamic cancer therapy, Au nanomaterials are used as carriers for photosensitizers, or are photosensitizers themselves. Upon specific wavelength light radiation, they produce reactive oxygen species that induce cell death [6, 7, 25]. Au nanomaterials are also attracting attention as radiosensitizers in X-ray radiotherapy. As a treatment it has the advantage of deeper penetration in tissues than the NIR light typically used for photothermal or photodynamic therapy. Au NPs absorb the X-rays and thus localize the X-ray damage by reactive free radicals and secondary electrons to tumour sites [25, 27, 28].

Even though bulk gold is inert, in the form of NPs it can display high catalytic activity for a variety of reactions. These include oxidations of olefins, alcohols and alkanes, hydrogenations, aminations and C–C coupling reactions. Au NP size as well as the material on which the particles are supported is critical for catalyst reactivity [1, 29, 30]. Supported Au NPs can catalyse important industrial reactions, such as hydrogen peroxide production, oxidative esterification of methacrolein to methyl methacrylate and hydrochlorination of acetylene to vinyl chloride monomer [31].

The performance of NPs for most of the applications presented above is affected by their size, shape and functionalization. For example, the size and shape of nanoparticle influences the LSPR shift [24]. The extinction coefficient of 5 nm Au NPs is much lower than that of larger Au NPs. When the size of Au NPs approaches the Fermi wavelength of electrons (<2 nm), molecule-like optical properties and size-dependent fluorescence appear [6, 15]. Large Au NPs have a longer electromagnetic field decay length and provide higher sensitivity; hence, they are more efficient at enhancing Raman signals [6]. Size, shape and surface chemistry affect nanoparticle circulation in the body and distribution to different organs. In general, NPs smaller than 6 nm are filtered by the kidneys, larger than 200 nm are retained by the spleen, while in the 30–200 nm range typically show better tumour accumulation.

Penetration of Au NPs through biological barriers depends on their size and surface charge [32–34]. Toxicity of NPs to cells is also size dependent, even though results are often contradictory [6, 7, 24, 35, 36]. For Au NPs used in catalysis, size critically influences their performance. Catalytic activity of Au NPs typically increases substantially as size decreases below 5 nm (e. g. carbon monoxide (CO) oxidation). However, selectivity to desired products can increase or decrease with nanoparticle size, depending on the particular reaction [37, 38].

4.1.2 Continuous synthesis of gold NPs

Since the performance of Au NPs depends on their size (and hence size distribution), shape, chemical composition and surface functionalization, controllable and repeatable processes for the synthesis of Au NPs are important to guarantee consistent performance. Most of the synthetic routes are performed in batch systems [39]. Batch processes are solution-phase synthesis techniques where reagents (precursor, reducing agent, capping agent) are mixed at controlled temperature. The precursor is reduced or decomposed generating atoms, the atoms nucleate and the nuclei grow into seeds and subsequently into NPs with desired characteristics. Batch-to-batch variations are problematic and a synthesis approach that gives uniform materials consistently is of paramount importance [40, 41]. However, if the kinetics of the synthesis processes are fast, mass and heat transfer can play an important role in the synthesis. Mass/heat transfer rates change with reactor size, limiting the control of the experimental conditions [42]. In conventional synthetic methods, the immediate addition of the reducing agent (and/or other reactants) leads to localized high concentrations (and in turn to concentration gradients) which can cause variable sizes and broad size distribution of the final particles, since these grow from nuclei produced at different times in places within the solution where the reactant concentrations are different. Such inhomogeneity can lead to coexistence of nucleation and growth, which can result in wide NP size distributions and poor control of shape and aggregation [39, 43]. Batch processes are often not amenable to scale-up, and they may not provide an appropriate balance between control of nanoparticle characteristics and productivity [39]. If promising laboratory results of Au NPs are to translate into commercial applications, larger scale reproducible manufacturing with satisfactory control of the NP desired characteristics needs to be developed [44].

Microreactors, which allow manipulating the fluid dynamics, heat transfer, and mixing at the sub-millimetre scale precisely, offer advantages in these cases. Due to the large surface-to-volume ratio and a decrease in diffusion paths, microreactors exhibit much better mixing, which plays an important role in monodisperse nanoparticle formation. In addition to this, because of the smaller volumes in microreactors, various parameters (temperature, pressure, residence time, etc.) can be controlled easily and safely, which can lead to precise control of the reaction with shorter response time [45].

The diffusive mixing in microreactors can reduce agglomeration as compared to conventional convective turbulent mixing [39]. Continuous microfluidic synthesis can make scaling to large production possible through parallel operation of multiple identical reactor units, reducing labour and time of processes [46–48]. It further allows easier automation, online monitoring of nanoparticle characteristics and use of closed loop control systems to achieve quality control [40, 49, 50]. Microfluidic systems offer the opportunity for easier integration of complex sequential processes, such as those required for the functionalization of Au NPs, which is a key step for biomedical applications [41].

Taylor dispersion in micro or millifluidic reactors can arise from the shear on the fluid caused by no-slip boundaries at the channel walls. This leads to a parabolic velocity profile, which generates a spread in the residence times of the fluid elements, and therefore of the NPs present in them, because the elements flowing near the channel axis move more quickly than those flowing near the channel walls. Taylor dispersion can increase polydispersity in channels where the residence time distribution (RTD) is wide. Fouling of the microreactors due to nanoparticle nucleation/growth/attachment on the wall material can also be an issue [51]. These disadvantages can be addressed by segmented flow microreactors, where the synthesis takes place in isolated droplets (behaving as moving batch reactors) protected by the segmenting fluid from the tubing wall [52–56]. Fouling and higher productivity can also be addressed by millifluidic systems (increasing channel dimension by an order of magnitude). Moreover, these devices are often cheaper and easier to clean, if the requirements for mass and heat transfer are not severe [41].

There have been various reviews on the preparation methods of Au NPs mostly from the viewpoint of chemistry routes [1, 34, 57–60]. Reviews in the use of microreactors for the synthesis of various types of inorganic NPs have been presented [39, 41–43, 50, 52, 53, 61–64] and some focus on Au NP synthesis using microfluidics [45, 65]. In this chapter, we aim at reviewing the current state of the art in flow synthesis of Au NPs from a reactor engineering point of view, highlighting the inherent differences of flow reactors from conventional batch reactors, as well as potential issues that may be encountered during the development of continuous processes for the production of this class of materials. This culminates to a design methodology that highlights key steps for the development of a manufacturing flow system for the synthesis of Au NPs. The proposed design procedure is based on a series of interconnected steps that emphasize the importance of an interdisciplinary effort between chemists, engineers and physicists, and is summarized in 10 main design rules.

4.2 Requirements for quality-by-design synthesis

Currently, the design of nanoparticle reactors strongly relies on a trial-and-error experimental approach, occasionally guided by design-of-experiments methods. Mathematical models for the syntheses based on first principles are rarely used to

design and optimize these reactors. This is in stark contrast with the design methodology adopted in the manufacturing of more conventional products, for which the principles, methods and models of reaction engineering (or more advanced approaches) are commonly employed. This *modus operandi* prevents, or at least complicates, the attainment of *quality-by-design*, where one aims to build quality into a product, instead of testing quality from a product. Theoretical models for particle syntheses would allow rationalizing nanoparticle reactor design and developing systems able to deliver products with the desired characteristics in a more robust and cost-effective manner, whilst building valuable process knowledge.

Due to the complexity of nanoparticle syntheses, which involve many physical and chemical concurrent phenomena, developing models for these systems is truly challenging. In addition to an accurate mechanistic description of a specific synthesis method, model development necessitates the knowledge of the kinetics of the reactions and processes (such as particle nucleation, aggregation and growth) involved in the synthesis as well as of the fluid dynamics in the reactor, which affects heat and mass transfer. Obtaining accurate kinetic information is particularly critical, but at the same time particularly difficult.

4.2.1 Characterization and kinetics of nanoparticle synthesis

In this section we introduce experimental techniques that are useful for the characterization of gold NPs. We first comment on the most commonly employed techniques, and then we focus on techniques useful for the quantification of NPs synthesis kinetics. This last point is of relevance for the development of flow reactors, as an optimized reactor design procedure is based on the knowledge of reaction kinetics [66]. In the last paragraphs we discuss the possibilities offered by flow systems for *in situ* synthesis monitoring, appealing features for both kinetics studies and process control.

Key parameters of interest in nanoparticle syntheses are product concentration (as in "conventional" chemical syntheses), as well as particle size and particle size distribution (PSD). Measurement of unconverted precursor or product yield is important too, not only for improved process performance but also because unconsumed precursor can keep reacting during storage if it is not removed. Other important parameters, which require at least qualitative information, include particle shape and surface properties. Hence, more than one experimental technique is generally required to fully describe nanoparticle synthesis processes.

Electron [67, 68] and scanning probe [69] microscopy have been widely employed to characterize particle size and shape. Au NP sizes and size distributions can be measured by dynamic light scattering [70], which however requires relatively monodisperse samples to render accurate measurements, and by differential centrifugation sedimentation, down to 2 nm in size [71]. For sub-2 nm gold NPs, whose structure could be altered by conventional techniques, such as transmission electron

microscopy, size can be measured by mass spectroscopy [72]. Average particle size and PSD can be measured via small angle X-ray scattering (SAXS) with a very low detection limit [73]. This technique also allows *in situ* measurements of the particle size evolution during the synthesis with resolution down to 2 nm, but synchrotron radiation is required [74–78]. SAXS also allows evaluating nanoparticle volume fraction in solution. Nanoparticle crystal structure and crystallite size can be determined by means of X-ray diffraction [79].

Gold concentration can be measured by means of several techniques. Very low detection limits can be achieved with inductively coupled plasma mass spectroscopy (ICP-MS) [80], which, with recent advances, can now also be used to determine NP number concentration and number size distribution (Single Particle ICP-MS) [81]. Voltammetric methods have been employed to determine gold concentration as well as NP number concentration [82–84]. After dissolution in strong acids, the elemental gold concentration (and in some cases the packing density of ligands) can be measured by means of atomic absorption spectroscopy [85] or optical emission spectroscopy [86–88]. Gold elemental analysis can also be performed with neutron activation analysis [89]; however, this requires complex instrumentation.

The oxidation states of gold can be obtained via X-ray photoelectron spectroscopy (XPS) [90] and X-ray absorption near-edge spectroscopy (XANES) [76–78, 91, 92]. Extended X-ray absorption spectroscopy fine structure can be used to gather information on crystal lattice properties and how these are affected by ligands [93]. The interactions between ligands and the gold NP surface can be studied by XPS [90, 94] and Fourier transform infrared spectroscopy [94, 95].

A simple yet powerful tool used for gold nanoparticle characterization is UV–vis spectroscopy. This technique offers the major advantage of requiring relatively cheap benchtop instrumentation, and is suitable for both *ex situ* and *in situ* measurements, which makes it very attractive for kinetic and mechanistic studies [74, 96–98]. Studies to link both particle size and Au(0) concentration to the solution UV–vis spectrum have been reported in the literature, where either the position of the LSPR and the extinction at this wavelength [88, 100] or the ratio between the extinctions at the LSPR wavelength and that at 450 nm [100] have been used. Hendel et al. demonstrated that the UV–vis absorbance at 400 nm (Abs_{400}) can be used to determine the $Au(0)^{\cdot}$ concentration in NP solutions, but pointed out that particle size, surface modification, or oxidation state can affect the measurement [101]. The type of ligands and the dielectric properties of the surrounding medium also significantly affect the UV–vis spectra; hence, this technique has to be correctly calibrated considering the ligands and solvent employed in the synthesis [102, 103]. UV–vis spectra can also be used to analyse the speciation of $HAuCl_4$ [97, 104], the most common gold precursor used for Au NP synthesis. Finally, this technique also allows assessing the quality of the gold precursor employed, whose spectra depend on its "age" and purity [73].

From a reaction engineering point of view, experimental techniques that are able to provide time-resolved data during the synthesis are of great interest, since they

permit quantifying reaction kinetics, which is an essential element for reactor design. Determining kinetics and rate laws is a major challenge in the field of nanoscience, both from an experimental and a theoretical standpoint, because these syntheses involve many concurrent physical and chemical phenomena belonging to synthetic chemistry, colloidal science and particle technology. Experimentally, a complete description of the kinetics of these processes requires several techniques as well as a wide scientific background for the correct interpretation of the data gathered.

Generally, the theoretical framework used to describe the kinetics of the nucleation process in nanoparticle syntheses is the classic nucleation theory, developed by Becker and Doring [105] and later extended by Lamer and co-workers [107]. However, several studies demonstrated that many nanoparticle syntheses are not well described by this theory [107, 108]. In this sense, Zeng and Oxtoby stated that "nucleation theory is one of the few areas of science in which agreement of predicted and measured rates to within several orders of magnitude is considered as major success" [109]. Xia et al. appropriately described the current state of progress in the study of nanoparticle formation kinetics, stating that "at the current stage of development, it is not an exaggeration to say that the chemical synthesis of metal nanocrystals (as well as for other solid materials) remains an art rather than a science" [110]. Along the same line, Polte recently pointed out that "the main reason for this lack of knowledge was the absence of reliable experimental information about the particle growth process, in particular of the particle size and concentration during the growth process" [111].

Some of the characterization methods presented above have been used *in situ* in batch systems to obtain mechanistic/kinetic information. Polte and co-workers [75, 76, 78, 97], employed SAXS combined with XANES to provide time-resolved average particle size, relative PSD standard deviation and gold oxidation state for the classical Turkevich synthesis in a wide parameter space. Abecassis et al. employed similar techniques to study the evolution of the PSD and of the Au oxidation state during different $NaBH_4$-based synthetic routes [74, 77]. Comparison between the total amount of Au(0) present in the solution (obtained by XANES) and the amount of Au(0) inside the NPs (obtained from SAXS) showed that a measurable amount of Au (0) existed transiently as monomers, suggesting burst nanoparticle nucleation. They further showed that ligands affect reduction kinetics and nucleation rate, and thus indirectly also NP growth. A model including reduction kinetics, nucleation and growth rates enabled the fitting of NP size and concentration time evolution. UV–vis spectroscopy was used by Hendel et al. to track the reduction of Au(III) to Au(0) in real time by measuring the Abs_{400} during the synthesis [101]. The data acquired via UV–vis spectroscopy were consistent with the experimental observations obtained by SAXS. Luty-Blocho et al. and Paclawski et al. used UV–vis spectroscopy and dynamic light scattering [112, 113] to quantitatively study the kinetics of the $HAuCl_4$ to $HAuCl_{4-x}(OH)_x$ reaction, which plays an important role in several Au NP synthetic routes [97]. A rate law for Au NP formation, according to a Finke-Watzky model (slow

nucleation, fast autocatalytic surface growth) [108], was formulated and utilized to design a microfluidic reactor system and select suitable operating conditions for the synthesis of Au NPs by glucose reduction. Georgiev et al. [69] studied the kinetics of the gold NP synthesis by the Turkevich method employing time-resolved UV–vis spectroscopy, as well as *ex situ* atomic force microscopy and obtained rate constants for a Finke-Watzky model that were similar for both techniques. However, *ex situ* measurements may give "drying" artefacts during the sample preparation, affecting the precision of the data acquired. As a consequence, the development of time-resolved *in situ* measurement techniques is one of the bottlenecks for the acquisition of reliable kinetic data. In this regard, interesting opportunities are offered by liquid phase transmission electron microscopy [114, 115] and cryo-transmission electron microscopy [116].

Flow systems allow also *in situ* characterization, with the added advantage that, since real time is replaced by space time (i. e. reactor location), information at very short reaction times can be obtained. In addition, in-line monitoring by optical techniques can be easily implemented. This feature is attractive, as it opens up possibilities in reaction kinetic studies, also enabling simple implementation of process control loops. For instance, McKenzie et al. combined SAXS and UV–vis spectroscopy in a microscale flow system (Figure 4.1a) for *in situ* monitoring of PSD and UV–vis absorbance of sub-5 nm gold NPs at different concentrations, with results that correlated well with *ex situ* TEM and UV–vis measurements [117]. Watt studied the effect of seed age on gold nanorods formation by using a microfluidic system with in-line UV–vis–NIR spectroscopy [118], which was combined with *ex situ* SAXS measurements to observe the change of the nanoparticle population during aging. However, UV–vis is not suitable if there is no LSPR band [119]. Polte et al. employed *in situ* SAXS in combination with XANES to monitor the synthesis of Au NPs with size between 0.8 and 2 nm (Figure 4.1b) [76]. A static micromixer was used to provide homogeneous mixing between gold precursor and $NaBH_4$, and then the products were detected by SAXS in a flow cell. As $NaBH_4$ is quite a strong reducing agent, the reaction finished within 100 ms and increasing residence time did not change the size. The work suggested a two-step mechanism of gold nanoparticle formation: a rapid conversion of the ionic gold precursor into metallic gold nuclei, followed by particle growth via coalescence of smaller entities. Similarly, Tofighi et al. used *in situ* XANES assisted by a microfluidic silicon chip to study the early reaction stages of the polyvinyl pyrrolidone (PVP)-stabilized Au NP synthesis by $NaBH_4$ reduction (Figure 4.1c) [120]. The chip allowed the beam focusing on different positions along the microchannel to track the reaction. It was observed all the gold ions were reduced to Au(0)· within the first 10 ms. Yue et al. described how to monitor the synthetic process of Au NPs with in-line UV–vis in segmented flow by a cross-type flow-through cell (Figure 4.1d) [121]. However, the main difficulty to apply in-line UV–vis on a segmented flow system is that the detection limit could be affected by the background from the carrier fluid and reflection/scattering from the

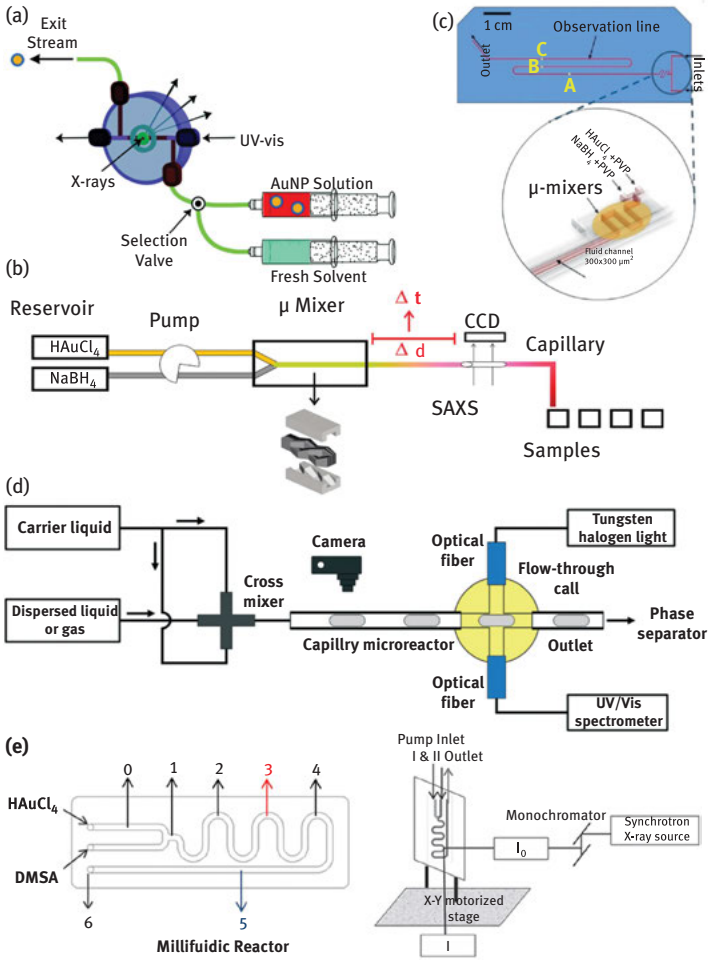

Figure 4.1: (a) Schematic of microscale flow system with a specially designed cell for *in situ* SAXS and UV–vis measurement of nanoparticle size distribution (reprinted with permission from Ref. [117]. Copyright 2010, American Chemical Society). (b) Experimental setup with flow cell for *in situ* SAXS (reprinted with permission from Ref. [76]. Copyright 2010, American Chemical Society). (c) Schematic illustration of microfluidic chip with different measuring points for *in situ* XAS; insert is the schematic of micromixer employed (adapted from Ref. [120]. with permission of The Royal Society of Chemistry, https://doi.org/10.1039/C7RE00114B). (d) Experimental setup for *in situ* UV–vis monitoring of reaction in segmented flow (adapted from Yue et al., Copyright 2013 Royal Society of Chemistry, Microreactors with integrated UV/Vis spectroscopic detection for online process analysis under segmented flow, https://doi.org/10.1039/C3LC50876E, https://creativecommons.org/licenses/by/3.0/legalcode) [121]. (e) Experimental design of millifluidic chip for *in situ* XAS monitoring at different locations along the channel (reprinted with permission from Ref. [122]. Copyright 2013, American Chemical Society).

slug curved surfaces. Krishna et al. used a millifluidic device for time-resolved mapping of the Au NP size evolution in growth (Figure 4.1e) [123]. The work identified the formation of stable gold sulphide NPs when chloroauric acid and meso-2,3-dimercapto succinic acid were mixed in the millifluidic reactor. The gold nanostructures formed deposited at the channel and were subsequently reduced by flowing $NaBH_4$. The reduction was monitored with XAS spatially with a time resolution of 5 ms.

4.2.2 Mathematical modelling of nanoparticle synthesis

We have shown how a wide variety of experimental techniques are required to characterize nanomaterial synthesis kinetics. Similarly, a variety of modelling techniques can be adopted to describe nanoparticle syntheses and extract useful kinetic information. These techniques differ in the level of detail that can be captured, and accordingly in the computational cost of the numerical simulations. Modelling techniques used to describe processes occurring in nanoparticle syntheses range from quantum chemical calculations (e. g. Density Functional Theory) to molecular dynamics, Brownian dynamics and Monte Carlo simulations. A detailed review of the applications of these techniques in describing nanoparticle structures is provided in Barnard [124]. The modelling approaches just mentioned are powerful tools for describing in detail "single" nanoparticle synthesis aspects, like precursor reduction [124], particle growth [125], interaction of nanoparticle surfaces with other molecules [126], crystal structure and stability of nanoclusters [127]. However, they cannot be used to model the entire nanoparticle synthesis, since this would be computationally too demanding. A tool that fits the need of both accuracy and fast computation, and which is thus useful for process development, is population balance modelling (PBM). A population balance equation (PBE) is an equation that allows describing the evolution of the nano-PSD during the synthesis (even though it cannot capture other details, such as crystal structure or particle morphology).

PBM is widely used in reaction engineering [128] for the rational design of polymerization [129–131] and crystallization [132–134] reactors. It has also been used to describe the process of nanoparticle formation [136–138], in particular semiconductor nanoparticle synthesis, both in batch [138] and in flow reactors [139, 140]. The PBM thus seems to be an approach best suited to rationalize the design of nanoparticle synthesis reactors and achieve quality-by-design.

If we consider a batch reactor, in which the solution is assumed to be perfectly mixed, so that all the properties, such as concentration and temperature, are spatially uniform, the PBE describing the NPs evolution during the synthesis can be written as:

$$\frac{\partial n(v,t)}{\partial t} = g\delta(v - v_{\min})$$

$$+\frac{1}{2}\int_{v_{\min}}^{v}\alpha(v-v',v')n(v-v',t)n(v',t)dv'-n(v,t)\int_{v_{\min}}^{+\infty}\alpha(v,v')n(v',t)dv'+G,$$

where $n(v,t)$ is the number density function defined so that $n(v,t)dv$ yields the number of particles with volume in the infinitesimal range dv about the value v at time t. This function is thus closely related to the PSD. The first term on the right-hand side of the equation models nucleation, with g being the nucleation rate and $\delta(v-v_{\min})$ a delta function centred at the nuclei size $v_{\min}$ (here it is assumed that all nuclei share the same size). The second and third are generation and consumption terms, respectively, that model particle agglomeration, with α being the agglomeration kernel. The last term represents particle surface growth. In general, these terms (in particular g and G) depend on the concentration of the various precursors present in the system and on the physicochemical properties of the latter. From this equation we observe how different physical phenomena contribute in making the PSD change. For example, both agglomeration and surface growth cause an increase in the average particle size. Furthermore, one must keep in mind that the evolution of the PSD depends on the concentration of the precursors, so that the PBE is in general coupled with the material balances of all the other species involved in the synthesis (for instance, through g and G). Consequently, the mathematical model can be solved only if the rates of all the reactions are known and kinetic expressions for nucleation (via the term g), aggregation (via the term α) and growth (via the term G) are available. Hence, a significant amount of kinetic information is required, which cannot be obtained merely via the experimental acquisition of data on the PSD evolution.

A PBM for the Brust-Schiffrin method [141] shows how it is possible to improve the nanoparticle quality based on theoretical findings, significantly reducing the effort in reaction optimization. The model was based on a continuous nucleation – growth – capping mechanism, which indicated that, if the reaction conditions were kept constant, the particles born at different times through continued nucleation would grow to the same size before being capped. This is in contrast to the perception that continued nucleation is the main reason for poor PSD control. The authors were in fact able to propose a modified protocol based on their model, which led to an improvement of the Au PSD from 2.0 ± 0.6 nm to 1.7 ± 0.3 nm.

On the other hand, the work from Kumar et al. on the Turkevich synthesis [142] shows how significant effort has to be put in the understanding of the mechanism behind the synthesis. Despite the fact that this model qualitatively describes several aspects of the synthesis observed experimentally (in particular particle size plateauing for high citrate-to-chloroauric acid ratio values), Agunloye et al. showed that it poorly predicts experimental data from the literature [143]. This is most probably due to an inaccurate description of the synthesis mechanism. While Kumar and co-workers employed the Turkevich organizer theory [144], recent

work from Polte's group showed experimental findings supporting a different mechanistic route [97].

4.3 Review of research on gold nanoparticle flow synthesis

4.3.1 Gold nanoparticle synthesis in single-phase flow systems

4.3.1.1 Microfluidic reactors

Most microfluidic reactors are made using microfabrication methods and have characteristic dimensions in the order of hundreds of microns. However, the use of capillary tubes is also gaining interest owing to their simplicity and low cost. An important aspect for the application of continuous flow in the manufacturing of nanomaterials is its production capacity. Hence, for the sake of convenience, in this chapter flow systems with characteristic size (such as diameter) smaller than 1 mm are referred to as microfluidic reactors, while those with larger size (up to some mm) are referred to as millifluidic reactors. For Au NP synthesis, the most common microfabricated reactor materials are Si, glass and polydimethylsiloxane (PDMS). Glass and silicon not only involve special working conditions (clean room), but may also require careful sealing procedures, particularly for high temperature/pressure operation. Capillaries and tubes made of silica, polytetrafluoroethylene (PTFE) are common, while polyether ether ketone (PEEK), polyethylene and Tygon have also been used.

Among all the chemistry routes for Au NP synthesis, the Turkevich method has been the most popular [60] for synthesizing citrate-capped Au NPs. It was first proposed by Turkevich [144] in 1951, and produced around 20 nm Au NPs by adding trisodium citrate dehydrate quickly into a boiling $HAuCl_4$ solution under vigorous stirring. The mechanism was described as "seed-mediated growth" by Wuithschick et al. [97] who proposed a fast nucleation and a subsequent slow growth stage, as the gold ions preferentially bind onto the existing solid gold surface with lower surface potential [145]. On the basis of the Turkevich method, various researchers sought to improve this method [96, 146–151] or substitute the reducing agent (e. g. ascorbic acid [152] and tannic acid [153]) or capping agents [154–156] to achieve smaller/different particle size or narrower size distribution. For the synthesis of sub-5 nm Au NPs, sodium borohydride ($NaBH_4$) is the reducing agent most frequently used, having far higher reducing ability than citrate to reduce gold ions to metallic atoms (order of magnitude of milliseconds [76]) To limit the growth of particles, strong capping agents such as thiols in the Brust-Schiffrin method [157] are used during $NaBH_4$ reduction.

In single-phase microfluidic systems, the flow pattern is usually laminar, characterized by low Reynolds number [42]. Thus, mixing only occurs at the interface between miscible streams by molecular diffusion. This characteristic is attractive for some synthetic processes which need precise control. Citrate-capped Au NPs are usually synthesized by the Turkevich method for around 30 min under elevated temperature. Singh et al. produced citrate-capped Au NPs with lower reaction time

at room temperature by substituting citrate with the strong reducing agent $NaBH_4$ in the microreactor [156]. The laminar flow forming in the microreactor played an important role to slow down mixing and avoid the uncontrollable reaction owing to the high conversion rate of $NaBH_4$. On the other hand, for slower reducing agents efficient mixing is beneficial. Jun et al. studied the size control of Au NPs produced by ascorbic acid, by comparing different mixers. Similar size and size distribution were obtained with both microfluidic butterfly-shape and millifluidic compressed-tubing mixers (Figure 4.2), as long as the flow rate was sufficient to attain efficient mixing [158]. Sufficiently high flow rates could guarantee fast mixing, but too high flow rates did not allow enough time for the reaction to complete.

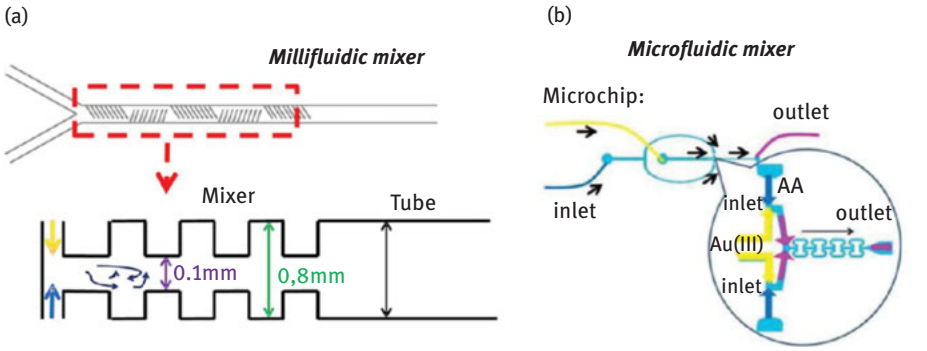

Figure 4.2: Schematic of different mixers used for Au NPs synthesis by ascorbic acid: (a) compressed Teflon millifluidic mixer and (b) butterfly microfluidic mixer (reprinted with permission from Ref. [159]. Copyright 2012, American Chemical Society).

Shalom et al. adapted the Brust-Schifrin method to a flow system by mixing a prepared thiolate polymer and aqueous $NaBH_4$ in a radial interdigitated mixer (Figure 4.3a) [159]. The reagents passed through a circular channel and were then split into eight streams flowing towards the centre of a mixing chamber, while the outlet was in the centre of the chamber. For the same gold-thiol ratio (e. g. 2), the size and standard deviation in the microfluidic reactor were smaller (2.9 ± 0.6 nm) than those in batch systems (4.9 ± 2.1 nm). Tsunoyama et al. used a similar mixing approach with a multi-laminated mixer (from IMM) to improve mixing (Figure 4.3b) [160]. With $NaBH_4$ as reducing agent, they produced PVP-stabilized sub-2 nm Au NPs with high monodispersity, which showed higher catalytic activity in aerobic alcohol oxidation than Au NPs prepared in a batch reactor. Using the same micromixer, Luty-Błocho et al. studied the effect of flow rate on Au nanoparticle synthesis. Increasing the flow rate led to smaller polyvinyl alcohol (PVA)-capped Au NPs in the range of 1.5–3 nm when using ascorbic acid or $NaBH_4$ as reducing agent [161]. Interestingly, batch processing resulted in sediment formation after 1 h for the ascorbic acid system.

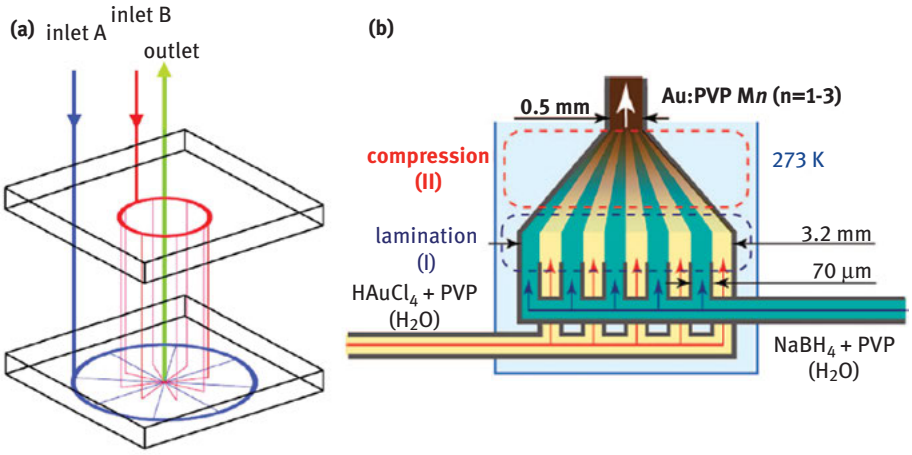

Figure 4.3: (a) Schematic of radial interdigitated mixer used for Au NPs synthesis by $NaBH_4$ (reprinted from Materials Letters, 61(4), Shalom et al., Synthesis of thiol functionalized gold nanoparticles using a continuous flow microfluidic reactor, 1146–1150, Copyright 2018, with permission from Elsevier) [160]. (b) Schematic of the multi-laminated mixer used for Au NPs synthesis by $NaBH_4$ (reprinted with permission from Ref. [161]. Copyright 2008, American Chemical Society).

For the $NaBH_4$ system, particles of similar sizes were obtained (~1.5 nm), but in the batch reactor much larger ones (~2 µm) were also produced.

A glass-silicon microreactor with three mixing zones of split-and-recombine type allowing the consecutive addition of reducing agent solution containing ascorbic acid and Fe(II) and three modifier solutions (citric acid, sodium metasilicate and PVA) was utilized to synthesize Au NPs [162]. Wagner and Köhler improved this glass/silicon reactor with eight split-recombine units (Figure 4.4a) which could provide improved RTD and used it to synthesize PVP-capped Au NPs with sizes between 5 and 50 nm by ascorbic acid reduction [163]. Au NPs with coefficient of variation (CV) two times smaller than that in a conventional batch reactor was achieved and smaller Au NPs were obtained at high flow rates, high concentration of the reducing agent or stabilizer and high pH. In a subsequent design, residence loops were added to allow for multi-step addition of the reagents and reduction of the risk of fouling (Figure 4.4b) [164]. They synthesized 4–7 nm Au NPs using $NaBH_4$ as the reducing agent. The Au NP size could be reduced by decreasing the reactant concentrations.

Sugano et al. developed a microreactor system comprising a Y-mixer and two piezoelectric valveless pumps to achieve pulsed mixing of chloroauric acid and trisodium citrate at room temperature (Figure 4.5) [165]. The switching frequency controlled the thickness of the pulsed layers, the square of which has a proportional relationship with the diffusion time. The mixing time at 100 Hz was short enough as to reduce the CV of the PSD to ~10 % for Au NPs of ~40 nm mean size.

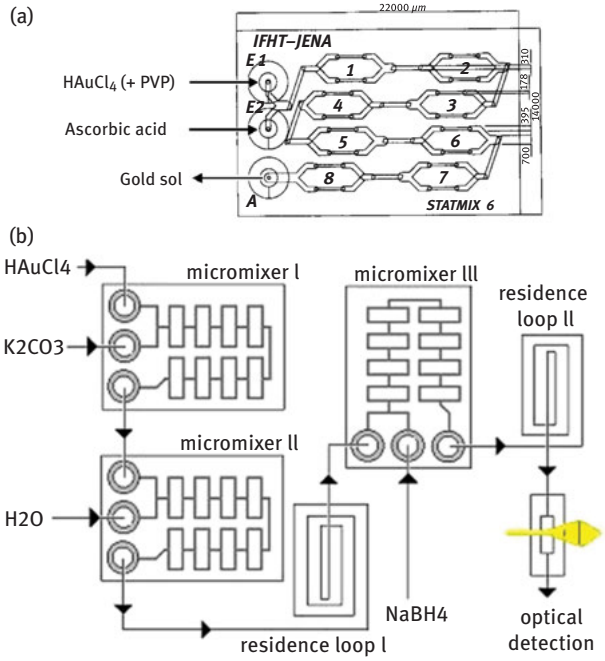

Figure 4.4: (a) Schematic of the reactor with split-and-recombine mixers used for synthesis of Au NPs by ascorbic acid (reprinted with permission from Ref. [164]. Copyright 2005, American Chemical Society). (b) Microreactor system with micromixers and residence loops used for synthesis of Au NPs by $NaBH_4$ (reprinted from *Chemical Engineering Journal*, 135, Wagner et al., Microfluidic generation of metal nanoparticles by borohydride reduction, S104–S109, Copyright 2008, with permission from Elsevier) [165].

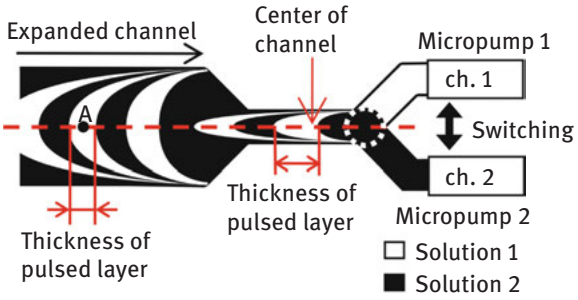

Figure 4.5: Y-shape pulsing mixer used for synthesis of Au NPs by trisodium citrate (reprinted by permission from Springer Customer Service Centre GmbH: Springer, *Microfluidics and nanofluidics*, Ref. [165], Sugano et al., Copyright 2010).

Verma and Kumaran formed co-axial flow in a microchannel ($H \times W$: 100 µm × 1.5 mm) so that the gold precursor (chloroauric acid) was surrounded by the reducing agent (tannic acid). As the Reynolds number increased, the flow regime

transitioned from laminar to turbulent. At high Reynolds number (up to ~350) the PSD could be controlled better, while the mean particle size, between 4 and 7 nm (achieved at different molar ratios of tannic acid to chloroauric acid) was not significantly affected by mixing conditions [166]. Bandulasena et al. also used a co-axial flow setup operating at laminar flow with an injection orifice diameter of the inner tube between 100 and 240 µm (Figure 4.6) [167]. The particle size of PVP-capped Au NPs produced by ascorbic reduction decreased from ~135 nm to ~50 nm by decreasing the injection orifice diameter (which increased the mixing efficiency), increasing the flow rate of the ascorbic acid stream and increasing the pH (which enhanced the reducing power of ascorbic acid). However, polydispersity increased with increasing the flow rate and the pH of the ascorbic acid stream.

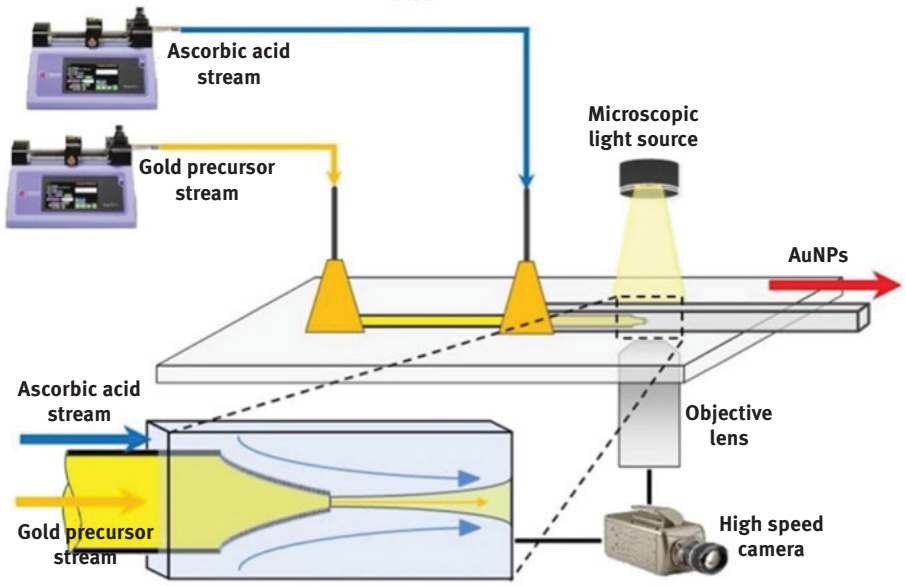

Figure 4.6: Schematic of the co-axial microfluidic setup with round capillary orifice inside a square microchannel used for Au NPs synthesis by ascorbic acid (adapted from Bandulasena et al., Copyright 2017 Elsevier, https://doi.org/10.1016/j.ces.2017.05.035, http://creativecommons.org/licenses/by/4.0) [167].

Baber et al. utilized a co-axial flow reactor comprised of an outer glass tube (2 mm I.D.) and an inner glass tube (0.8 mm I.D.) to bring in contact chloroauric acid and trisodium citrate, while avoiding fouling. This was followed by an ethylene tetrafluoroethylene-coiled flow inverter with 0.75 mm I.D., which helped to improve the RTD. Au NPs with minimum size of 17.9 ± 2.1 nm were synthesized at 80 °C (Figure 4.7) [168].

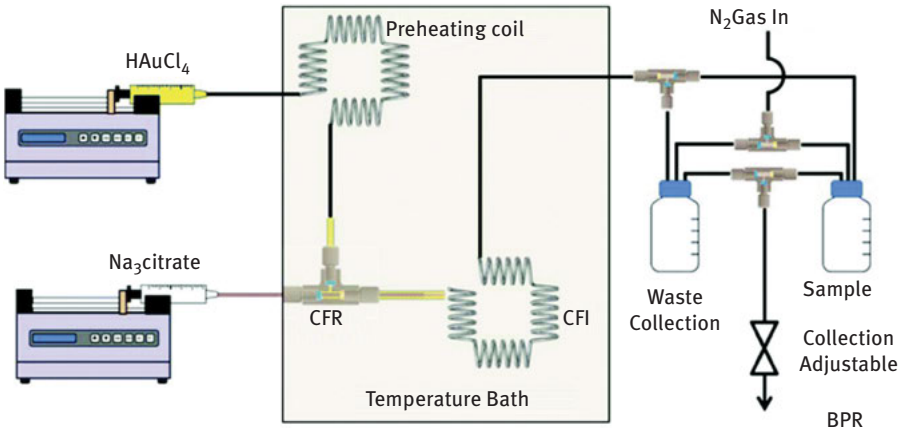

Figure 4.7: Schematic of the experimental setup for Au NP synthesis by the Turkevich method comprising coiled flow inverter (CFI) for preheating, a co-axial flow reactor as a mixer, and another CFI as reactor (adapted from Baber et al., Copyright 2017 Royal Society of Chemistry, An engineering approach to synthesis of gold and silver nanoparticles by controlling hydrodynamics and mixing based on a co-axial flow reactor, https://doi.org/10.1039/C7NR04962E, https://creativecommons.org/licenses/by/3.0/legalcode) [168].

Yang et al. designed a vortex-type mixer in a three-layer microfluidic reaction chip (Figure 4.8) [169]. Using the new chip, almost complete mixing was achieved within 1 s, and 19–58 nm Au NPs were obtained by tuning the volumes of citrate and gold precursor for the Turkevich method.

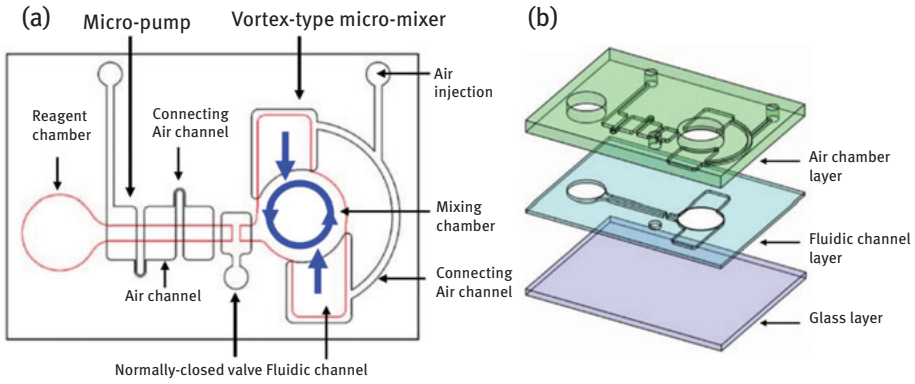

Figure 4.8: Components of three-layer microfluidic reaction chip with vortex-type flow field used for Au NPs synthesis by trisodium citrate (a) top view and (b) exploded view (reprinted by permission from Springer Customer Service Centre GmbH: Springer, *Microfluidics and Nanofluidics*, Ref. [170]., Yang et al., Copyright 2010).

Kitson et al. designed 3D printed serpentine reactors with 0.8 mm channels made of polypropylene (PP) to synthesize Au NPs [170]. Compared to the PDMS which is commonly used, PP is cheaper and the maximum material cost for one reactor was ca. $0.31. Even though fouling was observed on the surface of the reactor, this design is attractive because of the low cost for each reactor, which is disposable after one use.

The batch Turkevich method does not produce Au NPs <5 nm. However, Ftouni et al. produced ultra-small (i. e. <2 nm) Au NPs at residence time <50 s in a citrate-only system by taking advantage of efficient mixing and quick heating and quenching in a fused silica capillary (200 μm I.D.) [171, 172]. As the residence time was quite short and the product was quenched rapidly to terminate the reaction, no further growth after the quenching led to NPs with ultra-small size. Gomez-de Pedro et al. fabricated a ceramic microfluidic device based on low-temperature co-fired ceramics technology [173]. The shape of the three-dimensional serpentine structure caused advective patterns that enhanced the mixing. The reactor was used to synthesize 11-mercaptoundecanoic acid (MUA)-capped Au NPs. Pulsed dosing of $HAuCl_4$ solution to a continuous flow of $NaBH_4$, with a continuous downstream feed of an MUA solution, resulted in 2.7 nm Au NPs. Hydrophobic gold NPs have attracted less attention. Sugie et al. used a Y-mixer/PTFE microreactor assembly maintained at 25–60 °C to reduce $HAuCl_4$ in tetrahydrofuran solvent using organosilane as mild reducing agent and alkyl thiol (RSH) as capping agent [174]. Increasing residence time to over an hour led to the increase of the Au NP size from 4.3 to 8.7 nm.

Microfluidic systems have also been employed to form gold nanomaterials with different shapes. Kumar et al. used Br^- ions from cetyltrimethylammoniumbromide (CTABr) or HBr with citrate reduction to produce triangular gold nanoplates [175]. They implemented a Y-shape micromixer and a tubular PTFE tube with 0.9 mm internal diameter (I.D.) to tune the operational parameters (volumetric flow ratios, temperature and reagent concentrations) and improve the yield of triangular particles from ~25 % to ~51 %. Reducing the amount of citrate yielded a larger amount of polyhedral particles; this was attributed to the particle growth rate dominating the initial nucleation rates. Fu et al. developed a three-inlet micromixer and a subsequent PDMS microchannel (400 mm × 400 mm cross-section and 3 cm in length) for the synthesis of seed-mediated gold nanoplates [177]. The thickness of the nanoplates was tuned from 1 nm to a few nm by varying the flow rate. The nanoplates were rigid and flat when their thickness was >2 nm and had crumpled/rolled shapes when the thickness was ~ 1 nm. Sebastián et al. utilized a coiled PTFE tubing (0.76 mm I.D., Figure 4.9) to synthesize biocompatible gold nanorods (Au NRs) with a residence time of 10 min in continuous flow [178]. In order to circumvent toxicity issues of silver/CTABr that are typically used for Au nanorod synthesis, they employed lysine as capping agent with $NaBH_4$ as reducing agent. The presence of two amino groups in the lysine is critical for the anisotropic growth of the Au particles. By tuning the lysine concentration, Au nanorods with strong absorption in the near infrared (700–900 nm) were prepared.

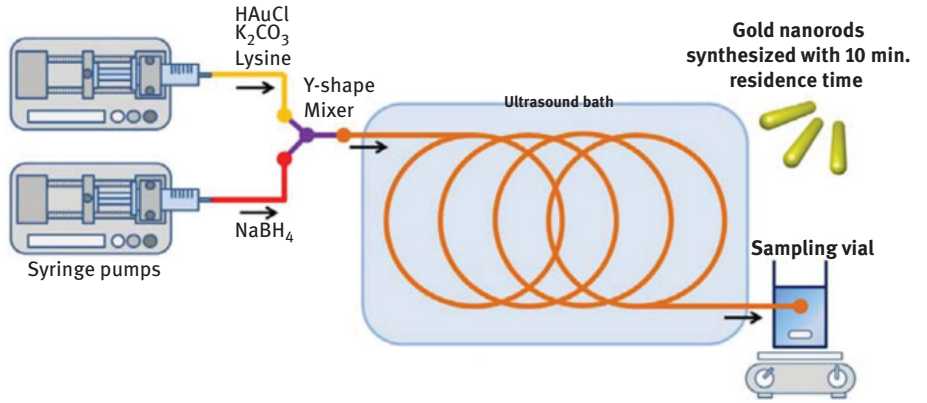

Figure 4.9: Schematic of continuous flow setup Au NRs synthesis via $NaBH_4$ reduction with residence time of 10 min (adapted from Ref. [178], with permission of The Royal Society of Chemistry, https://doi.org/10.1039/C2CC32969G).

Ishizaka et al. made use of continuous flow to tune the pH of the gold precursor by adding the reagents stepwise (Figure 4.10) [178]. Glucose was used as an environmentally benign reducing agent. Star-shape Au NPs were synthesized when the pH was 6.9, which was not observed in batch systems under similar experimental conditions; nevertheless, the particles gradually coalesced into single round shape particles.

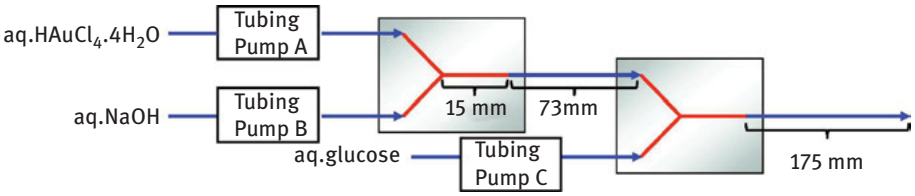

Figure 4.10: Schematic of multi-step addition in a microfluidic system for the synthesis of Au nanostars by glucose (reprinted from *Journal of Colloid and Interface Science*, 367(1), Ishizaka *et al.*, Dynamic control of gold nanoparticle morphology in a microchannel flow reactor by glucose reduction in aqueous sodium hydroxide solution, 135–138, Copyright 2018, with permission from Elsevier) [179].

An important issue during single-phase flow is the appearance of fouling on the microreactor wall. Wagner et al. observed gold precipitation on the wall of a glass microreactor, even though the synthesis was implemented carefully with small volume and short running time [163, 179]. They proposed various solutions to suppress fouling. Operation at high pH (~9.5) leads to negative charge on silicon surface because of the deprotonated Si–OH groups. As the citrate-capped gold NPs are also negatively charged, the electrostatic repulsion between product and tubing wall

prevented fouling. Another way is to reduce the wettability of the channel walls by turning the surface from hydrophilic to hydrophobic via silanization. Higher shear forces induced by increasing flow rate seemed also to help reduce fouling.

4.3.1.2 Millifluidic reactors

Because of potential fouling problems and their inherent small volume, it is difficult for microfluidic devices to provide gram-scale production [39, 45, 52, 62, 180]. Millifluidic reactors, which have one order of magnitude larger dimensions compared to microreactors, mitigate the risk of fouling blockages and depend less on expensive fabrication technologies [41]. Compared to batch synthesis, millifluidic devices can still provide satisfactory mixing (although this depends on the synthesis) and are more amenable to scale-up [158].

Lohse et al. proposed a millifluidic reactor system (Figure 4.11) comprised of simple components to improve the operation control compared to batch reactors, as well as to enable high-throughput synthesis at the gram-scale of functionalized gold NPs [181]. The reactants were mixed in a polyethylene (PE) Y-mixer (I.D. 1.79 mm), and the residence time was controlled by adjusting the length of the TYGON polyvinyl tubing reactor (I.D. 2.79 mm). The reactor could be integrated with online UV–vis absorbance spectroscopy analysis for product monitoring during synthesis, as well as flow NP purification techniques. Various functionalized (citrate, mercaptohexanoic acid and CTAB) spherical Au NPs with controlled sizes (4, 2 and 2–40 nm, respectively) were produced by $NaBH_4$ reduction. Furthermore, CTAB-stabilized gold seeds (2.0 nm) were mixed with a growth solution containing chloroauric acid, CTAB, silver nitrate, and ascorbic acid leading to Au nanorods with various aspect ratios and lengths of 15–50 nm.

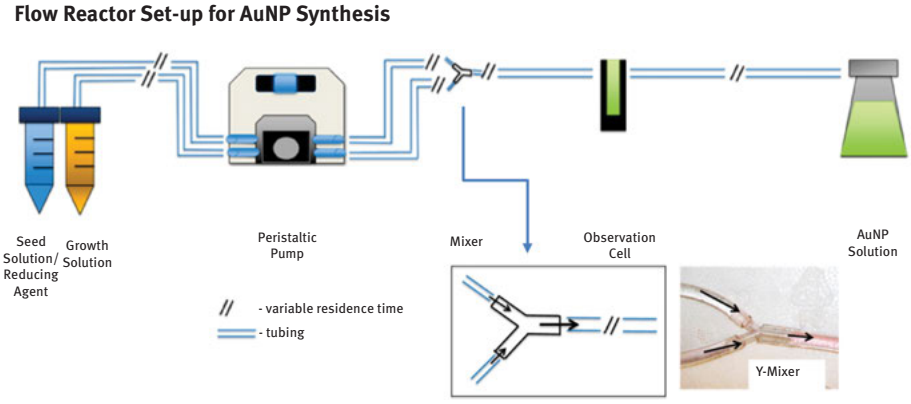

Figure 4.11: Schematic of a millifluidic reactor for Au nanomaterials synthesis by ascorbic acid (reprinted with permission from Ref. [182]. Copyright 2013, American Chemical Society).

Gomez et al. reported that the good quality of hollow Au NPs produced by galvanic replacement of cobalt NPs synthesized by $NaBH_4$ reduction in batch reactors could only be achieved with a volume up to 480 ml, as insufficient mixing limited the scale-up [182]. They achieved higher productivity by scaling up a continuous flow reactor from a PTFE tube with I.D. of 0.8 mm and length of 913 cm to millifluidic scale with 10 times higher throughput (I.D. of 1.6 mm, length of 3088 cm) (Figure 4.12). Moreover, multiple reaction stages, by adding new streams into the coils with T-junctions, and downstream processes (functionalization and

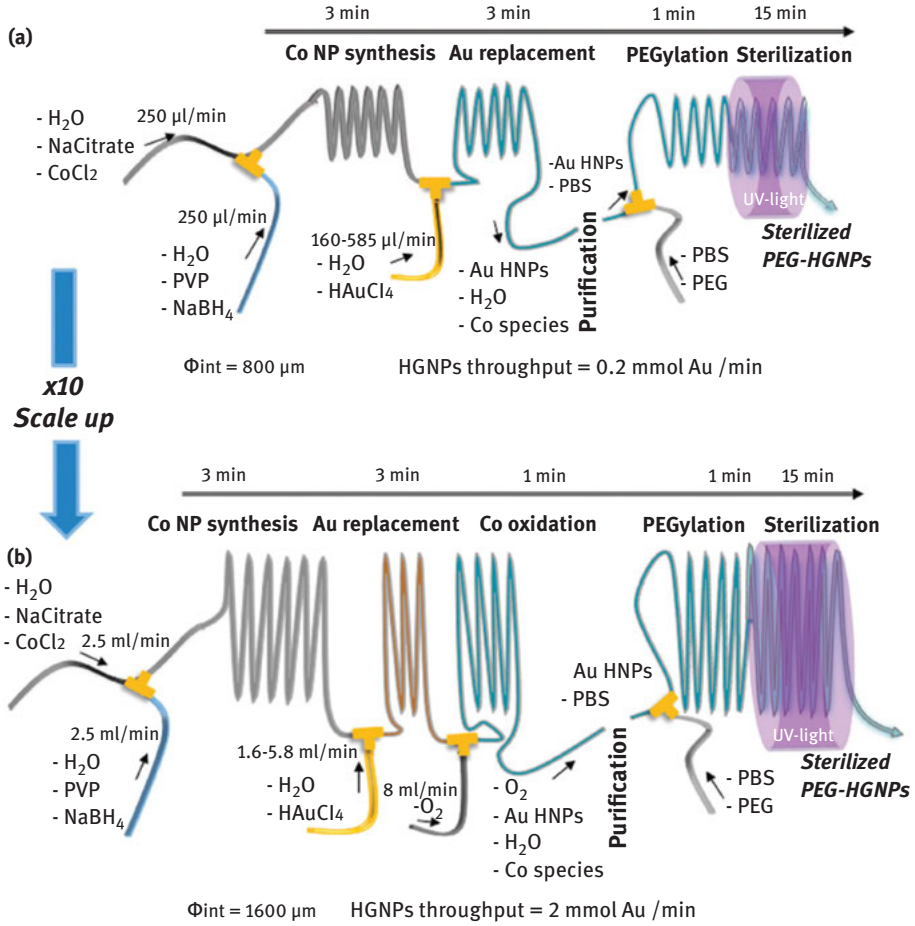

Figure 4.12: (a) Microfluidic setup with coiled capillary (I.D. of 0.8 mm) for the synthesis of sterilized PEG-capped hollow Au NPs by $NaBH_4$ through a galvanic displacement process. (b) Millifluidic setup with 10 times higher throughput (I.D. of 1.6 mm) than (a) (reprinted from *Chemical Engineering Journal*, 285, Uson et al., Continuous microfluidic synthesis and functionalization of gold nanorods, 286–292, Copyright 2016, with permission from Elsevier) [184].

sterilization) could be incorporated. Uson et al. utilized a similar setup based on PTFE tubing (I.D. = 1.016 mm) and PEEK Y-junctions to synthesize and functionalize Au nanorods in one continuous process [183]. The multi-addition of reactants allowed to separate and control – in a single stream – different stages of seed formation, nanorod growth and functionalization with poly(ethylene glycol)-methyl ether thiol (SH-PEG). Appropriate lengths of the tubing ensured the desired residence times (2–10 min) with a total residence time of 32 min. These short residence times eliminated detrimental effects associated with uncontrolled ageing-related processes observed in batch synthesis. The continuous system allowed a 100-fold reduction in the consumption of SH-PEG compared to a conventional batch reactor.

Bullen et al. used a rotating tube processor (RTP) with 6 cm I.D. and 30 cm in length with centrifugal force generating dynamic thin films 0.3 mm thick as the liquid moved along the rotating tube. The mixed reactant was delivered to a narrow channel processor (NCP) through jet feeds for longer residence time (Figure 4.13) [184]. Using this flow system, Au seeds were prepared with $HAuCl_4$/CTAB/acetylacetone and $AgNO_3$/CTAB/carbonate solutions in the RTP and grown to Au nanorods in the NCP. Long-term operation (19 days) was demonstrated with this system. Boleininger et al. [98] grew Au NRs from Au seeds and $HAuCl_4$/CTAB/ascorbic acid in short polyvinyl chloride (PVC) tubing (1 mm I.D.). The aspect ratio of the nanorods became smaller with a higher ratio of seed-to-growth solution or under higher growth temperature. Fouling was reduced by flushing polyethylene glycol before synthesis experiments. Different tubing materials were also tested. PVC, PTFE, PEEK and silicone tubes were filled with a growth solution containing gold precursor, ascorbic acid and CTAB for 3 h. There was no fouling observed in PVC and PEEK tubing, unlike PTFE and silicone.

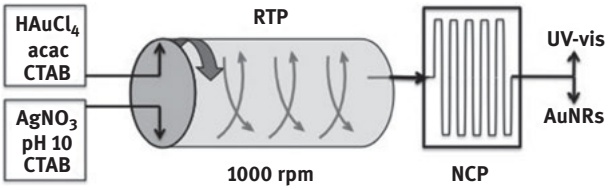

Figure 4.13: Schematic of the experimental setup for synthesizing Au nanorods by acetylacetone with a rotating tube processor (RTP) and a sequential narrow channel processor (NCP) (adapted from Ref. [185]. with permission of The Royal Society of Chemistry, https://doi.org/10.1039/C0CC05175F).

In addition to conventional heating for nanoparticle synthesis, there are other energy vectors that can be utilized. Sans et al. premixed the gold precursor and citrate at room temperature and then injected the solution into a coiled fluorinated ethylene propylene (FEP) tube (1.58 mm I.D.) placed inside a microwave cavity [185]. With this

setup, rapid feedback control during the experiments was obtained and hyperbranched gold nanostructures were discovered. Bayazit used a microwave-assisted flow system to synthesize Au NPs [186]. The 3.2 mm O.D. PTFE tube reactor produced Au NPs with average particle width 4–15 nm and aspect ratio ~1.4–2.2 after only 90 s residence time.

4.3.2 Gold nanoparticle synthesis in two-phase flow systems

4.3.2.1 Microfluidic reactors

Segmented (also Taylor or slug) flow induced by an immiscible fluid stream can provide better mixing via transverse convection, enhanced mass transfer and reduced dispersion [47, 53, 54, 56, 61, 187]. Furthermore, when the synthesis is conducted in the dispersed phase, the reactor wall is protected by a thin liquid film which helps to avoid fouling. However, some of the drawbacks are the necessity of downstream separation processes of the immiscible fluid streams, potential adsorption of NPs at the two-phase interface, keeping slugs uniform and avoiding their coalescence, and the difficulty of adding subsequent reactants in a uniform manner.

The slug length and slip velocity between the two phases are quite important parameters which determine the mass transfer between slugs [188]. In Cabeza et al.'s design (Figure 4.14) [189], the aqueous phase of gold precursor and $NaBH_4$ was

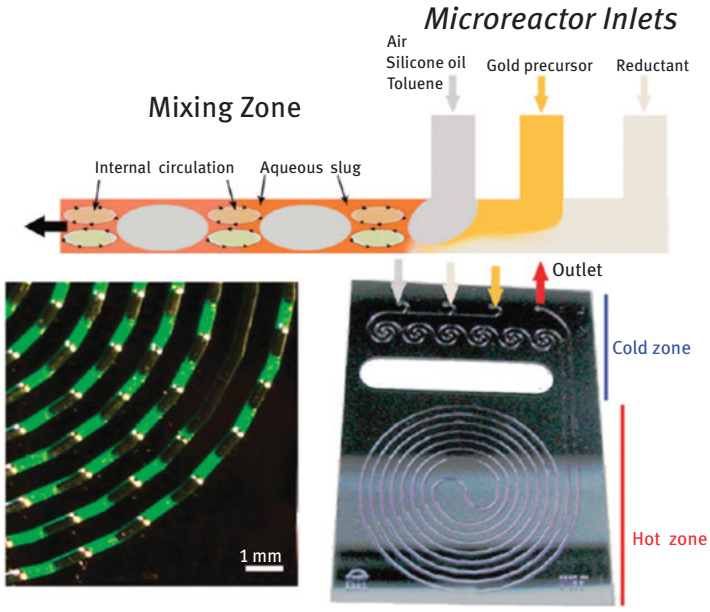

Figure 4.14: Segmented flow generation in a Si-glass microfluidic reactor used for Au NPs synthesis by $NaBH_4$ (reprinted with permission from Ref. [190]. Copyright 2012, American Chemical Society).

segmented by air, toluene or silicone oil inside a silicon microchannel ($H \times W$: 0.4 mm × 0.4 mm). The air-water two-phase flow resulted in the smallest and most monodisperse Au NPs with size 2.8 ± 0.2 nm, even though the reaction was in the continuous phase; this was attributed mainly to improved internal recirculation in the slugs. This system also led to the smallest amount of particle loss by interfacial absorption.

The same silicon microreactor was used as a hydrophilic reactor by Kulkarni and Sebastian Cabeza, and compared with a hydrophobic PTFE reactor (2.5 mm I.D.) for biphasic synthesis of Au NPs at the interface between an aqueous gold precursor and organic reducing agents (triethylamine, butyl amine, etc.) with CTABr as capping agent (Figure 4.15) [190]. The authors made use of the internal convection in segmented flow to renew the reactant at the interface in order to synthesize and grow the gold nanostructures. Nanoparticle preferential self-assembly at the water-oil interface by Pickering stabilization may have played a role in this synthesis [191]. Figure 4.15(d)–Figure 4.15(g) indicate different locations of particle accumulation for different wettability of tubing wall, which ultimately determined the nanoparticle size and shape. In hydrophilic microchannels the particles remained in the continuous aqueous slug and were located at the lower pressure region at the end of the slug [190]. When the particles moved to the end of one slug, they could be transferred to the next one along the film in the continuous phase while the droplet of the reducing agent would provide successive growth for these particles. The particles grew to form hexagonal bypyramidal shapes with a size of 42 nm. On the other hand, in hydrophobic microchannels the particles were trapped in individual droplets. The nuclei preferentially formed at the front-end of the droplet and then moved to the low-pressure end as their size increased. This movement enhanced the internal-mixing which led to higher nucleation rates and smaller final Au NPs (12 nm), whilst retaining the spherical shape.

Khan and Duraiswamy utilized N_2-aqueous segmented flow to synthesize Au NPs in a PDMS reactor with CTAB as a capping agent ($W \times D \times L$: 300 μm × 120 μm × 0.4 m) not only for better mixing, but also to stop the H_2 liberated from the $NaBH_4$ decomposition disrupting the flow (Figure 4.16) [192]. The evolved H_2 transferred to the N_2 bubbles leading to controllable stable flow. The authors showed that ultra-small Au NPs (<5 nm) could be synthesized with satisfactory quality to be used as seeds for CTAB-capped Au nanorod formation by off-chip synthesis.

Although internal recirculation in the slugs helps improve mixing, the mixing time scale may not be sufficient for nanoparticle syntheses which exhibit fast kinetics. In this case, winding microchannels can help break the symmetry of recirculation patterns and enhance mixing [193, 194]. While this is easily implemented in a planar microfabricated device, it is rather more difficult if one uses standard tubing. Thus, Zhang and Xia employed periodically pinched PTFE tubes with I.D. of 0.5 mm during droplet flow to decrease the mixing time from 15 to less than 1 s (Figure 4.17a), which led to more monodisperse Au NPs (Figure 4.17b) compared to the product under the same experimental conditions except without a pinched mixing zone (Figure 4.17c) [195].

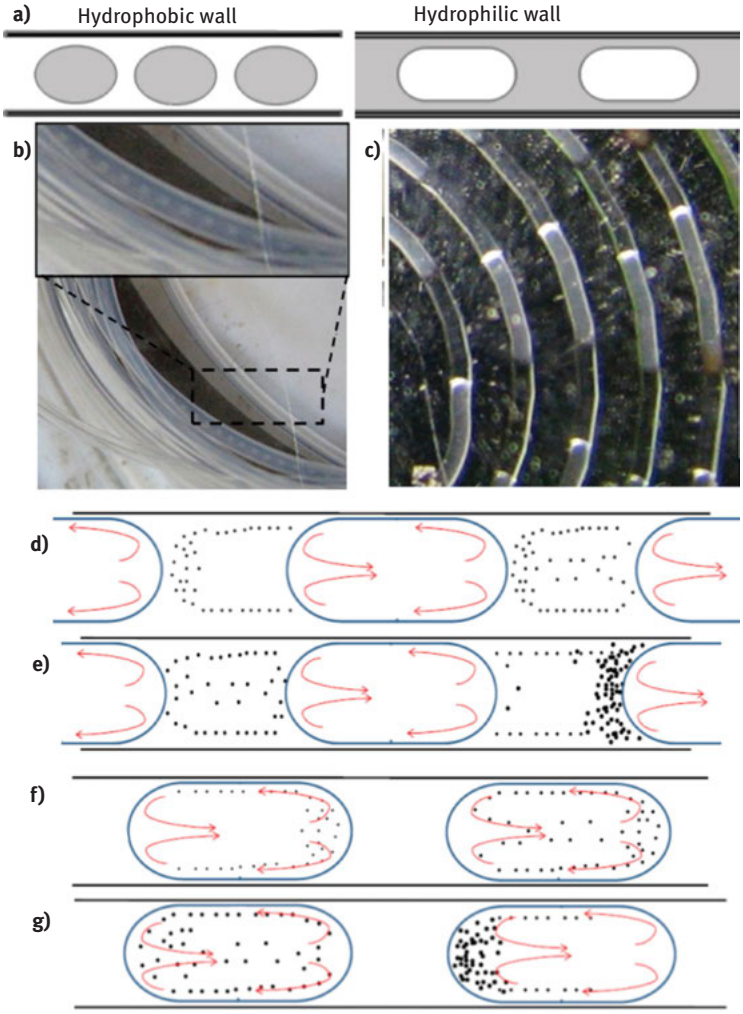

Figure 4.15: Schematic (a) and photograph (b) and (c) of flow patterns inside hydrophobic PTFE (left) and hydrophilic silicon-glass (right) reactors during slug flow (aqueous phase in grey and organic phase in white); (d) and (e) nanomaterial formation in hydrophilic reactor; (f) and (g) nanomaterial formation in hydrophobic reactor (reprinted with permission from Ref. [191]. Copyright 2017, American Chemical Society).

The flow patterns in the droplet-based systems depend on fluid properties [197]. Sometimes, a high concentration of the surfactant in seeded growth methods is necessary to guide the orientated growth or maintain the colloidal stability. These surfactant-rich reagents could increase the viscosity of the aqueous phase and change the interfacial tension to affect the droplet characteristics [197]. Duraiswamy and Khan employed a droplet-based microfluidic method during the surfactant-rich anisotropic

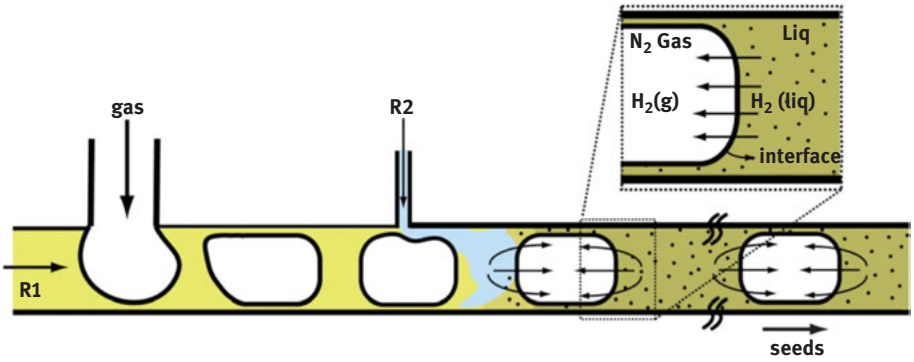

Figure 4.16: Schematic illustration of segmented N_2-liquid two-phase continuous flow for Au NPs synthesis by $NaBH_4$. The inset indicates the transport of H_2 from aqueous phase across to gas phase (adapted from Ref. [193]. with permission of The Royal Society of Chemistry, https://doi.org/10.1039/C2LC21198J).

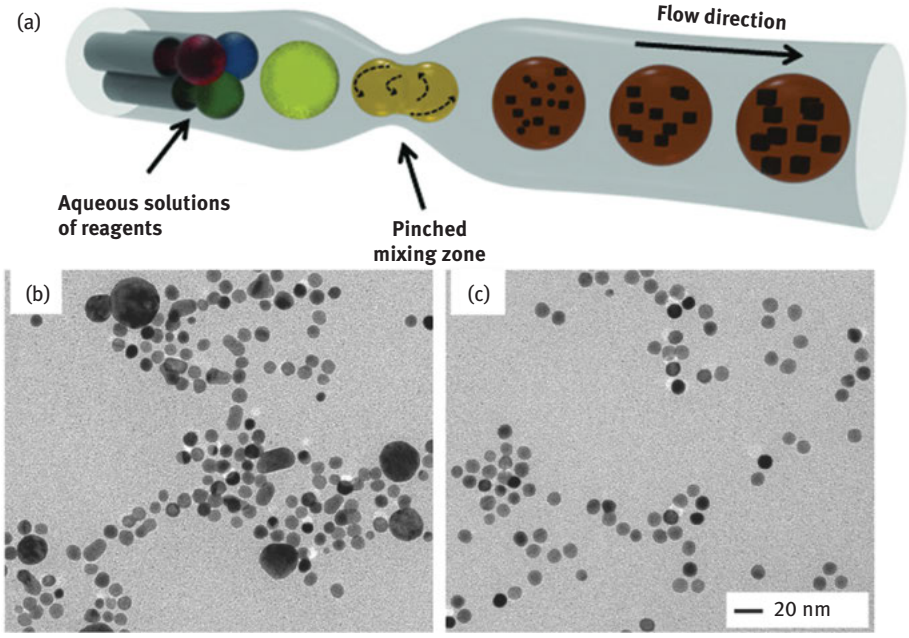

Figure 4.17: (a) Schematic of segmented flow inside 0.5 mm I.D. PTFE tube for Au NPs synthesis (b) with and (c) without pinched mixing zone (reprinted from Zhang and Xia, *Advanced Materials*, Copyright 2014 with permission from John Wiley and Sons) [196].

Au nanorod synthesis (Figure 4.18a) [198]. Three streams of gold seed solution, premixed gold precursor with capping agent (CTAB) and reducing agent (ascorbic acid) passed through one arm of the T-junction in a "flow-focusing" geometry and then

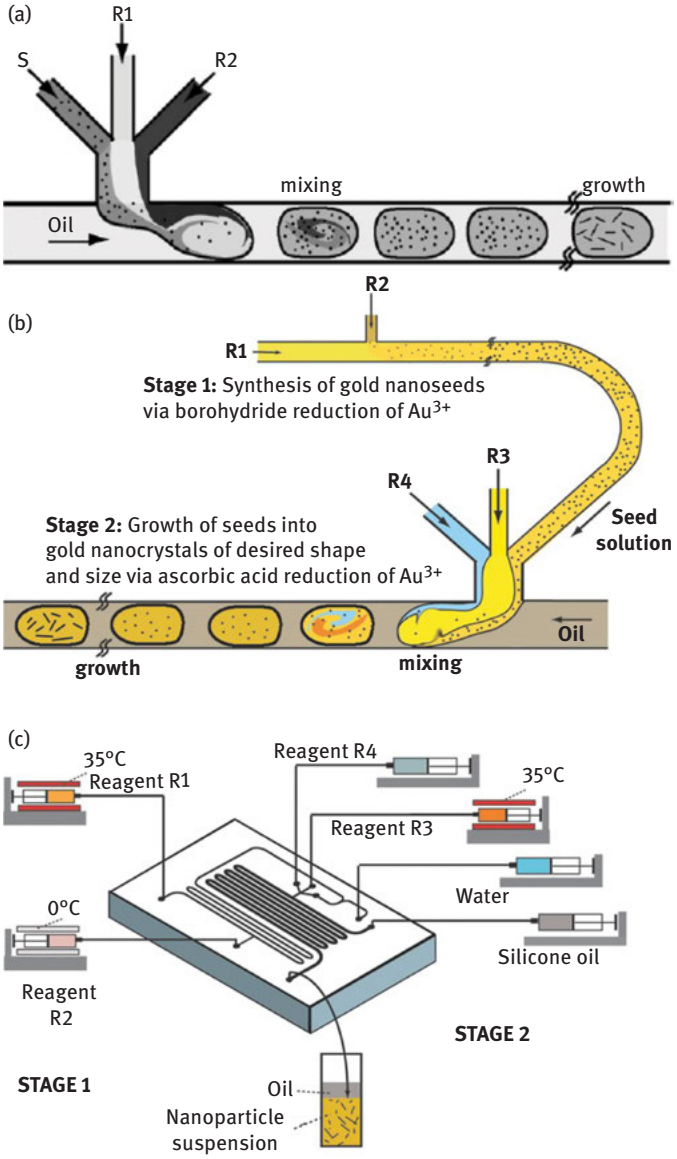

Figure 4.18: (a) Schematic of droplet-based microfluidic with three-arm mixer for aqueous droplet generation used for Au nanorod synthesis with ascorbic acid (reprinted from Duraiswamy and Khan, *Small*, Copyright 2009 with permission from John Wiley and Sons) [199]. (b) Schematic of the two-stage microfluidic method included gold nanoparticle seeds formation in Stage 1 and the growth of gold nanocrystals in Stage 2 and (c) the experimental setup (Reagent R1: aqueous mixture of gold salt and surfactant, Reagent R2: aqueous $NaBH_4$ solution, Reagent R3: aqueous mixture of gold salt, surfactant, and $AgNO_3$ and Reagent R4: ascorbic acid) (reprinted from Duraiswamy and Khan, *Particle & Particle Systems Characterization*, Copyright 2014 with permission from John Wiley and Sons) [200].

mixed with silicone oil to form homogeneous droplets inside a PDMS microreactor. By manipulating reagent concentrations and flowrates, Au nanorods with aspect ratio 2.3–2.7, as well as other shapes (e. g. cube, star, tetrapods), were obtained. Later, Duraiswamy and Khan combined the gold seed formation and the CTAB-capped nanorod growth together in a dual-stage continuous flow system (Figure 4.18b and Figure 4.18c). This time, the seed particles (<5 nm) were formed inside the PDMS microreactor channel ($W \times L$: 100 μm × 0.4 m) by $NaBH_4$ reduction and entered the subsequent growth section, which was a microchannel with $W \times L$: 300 μm × 0.45 m. Au nanorods with mean length ~35 nm and width ~12 nm were obtained [199]. The setup was further improved by adding a gas stream (N_2) to prevent the coalescence between droplets [200]. This microfluidic system was used to synthesize gold nanorods, but primarily gold-coated silicon-core particles by seeded growth.

Lazarus et al. employed a similar PDMS microreactor utilizing ionic liquid as solvent to synthesize Au NPs [201]. Ionic liquids, such as the 1-butyl-3-methylimidazolium tetrafluoroborate (BMIM-BF_4) used, are salts in liquid form which have poor-coordinated ions. The high nucleation rate caused by the high concentration in pure salt, low interfacial tension and chemical stability makes ionic liquids attractive for nanoparticle synthesis. With the aid of the microfluidic device to form homogeneous and stable droplets of ionic liquid, spherical Au NPs were smaller and with lower polydispersity (4.38 ± 0.53 nm) compared to those obtained in single-phase flow (6.25 ± 1.29 nm). Later, Lazarus et al. altered the synthesis by substituting the capping agent BMIM-BF_4 with 1-butyl-3-methylimidazolium bis-(trifluoromethylsulphonyl)imide (BMIM-Tf_2N) for greater stability and substituting the reducing agent $NaBH_4$ with BMIM-BH_4 for better solubility and prevention of sodium-containing by-products using a similar droplet-based microfluidic system and obtained 4.28 ± 0.84 nm Au NPs [202].

Taifur-Rahman et al. [203] utilized CO as a reducing agent in a membrane-based droplet microfluidic system to produce 10 nm Au NPs, as well as grow Au shells on gold nanoparticle seeds pre-attached on silica surfaces (Figure 4.19). The CO flowed

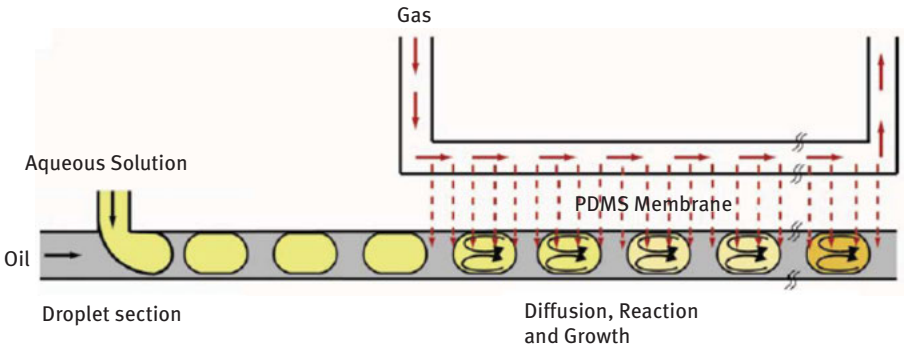

Figure 4.19: Schematic of the droplet microfluidic system with gas reducing agent (carbon monoxide) diffusing through a membrane (adapted from Ref. [204]. with permission of The Royal Society of Chemistry).

through a parallel gas channel ($W \times D \times L$: 100 µm × 124 µm × 21.8 cm) and could diffuse into the liquid channel ($W \times D \times L$: 300 µm × 124 µm × 91.5 cm) containing the water-fluorinated oil droplets flow via a PDMS membrane with thickness of 200 µm. Each droplet behaved as a reaction unit reacting with nearly equal amounts of CO with the same volume and good internal convection. The residence time could be controlled by the gas-liquid contact time. Calculations indicated that the CO mass transfer resistance in the liquid phase was the rate-limiting step. The mixing time (~0.1 s) was smaller by at least one order of magnitude than the residence time, enabling a controlled amount of the CO reducing agent to enter each droplet under shorter times.

Abalde-Cela et al. mixed an aqueous solution with a continuous phase of HFE-7500 fluid containing 2.5 % of Picosurf-1 surfactant for quick addition of ascorbic acid, which is critical for the synthesis of Au nanostars [204]. PDMS reactors with 100 µm × 75 µm or 80 µm × 75 µm T-junctions were utilized (Figure 4.20). The size of Au nanostars obtained was 170 ± 7.8 µm for a surfactant free synthesis and 90 ± 2.0 µm when PVP was utilized.

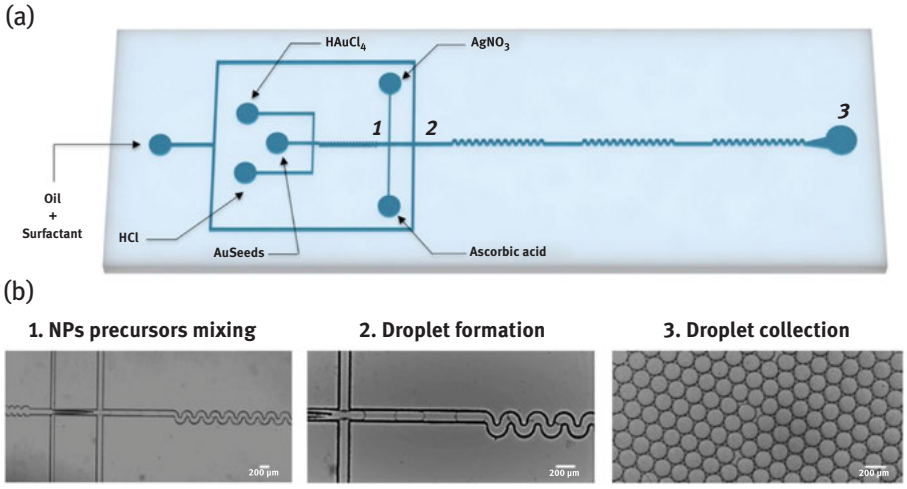

Figure 4.20: (a) Schematic and (b) optical images of a droplet microfluidic device to synthesize Au nanostars by ascorbic acid (adapted from Abalde-Cela et al., Copyright 2018 *Scientific Report*, https://doi.org/10.1038/s41598-018-20754-x, http://creativecommons.org/licenses/by/4.0) [204].

UV irradiation has been utilized to initiate the nucleation of NPs in segmented flow systems. Hafermann and Köhler used a solution of chloroauric acid, a photoinitiator and PVP that was exposed to a UV ray for a short period of time (30–300 ms) to induce nucleation followed by a growth section in the same 0.5 mm I.D. PTFE tube. Perfluoromethyldecalin was used as the segmenting fluid. In this system nucleation and growth could be spatially separated. The particle size was tuned between 2.5 and

4 nm by varying the composition of reactant solutions or the flow rate [204]. du Toit et al. synthesized citrate-capped Au NPs within heptane-water droplet flow using the Turkevich method [71]. UVC lamps were used to enhance the nucleation rate in a 0.8 mm I.D. glass capillary followed by FEP tube (1 mm I.D.) for controllable growth with conventional heating (Figure 4.21). By varying the UV intensity and growth temperature at an exposure time of 10 s, the nanoparticle size was tuned between 6.6 ± 0.8 nm and 36.1 ± 6.9 nm.

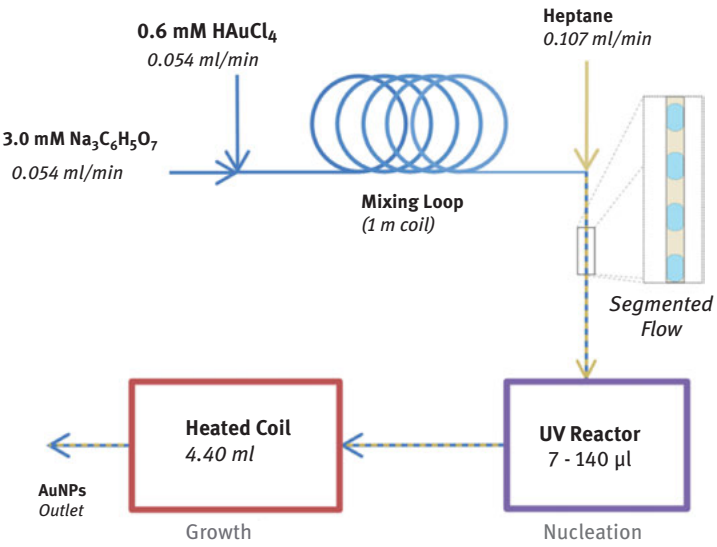

Figure 4.21: Schematic of continuous segmented flow for Au NPs synthesis with UV radiation by citrate (adapted from du Toit et al., Copyright 2017 Royal Society of Chemistry, Continuous flow synthesis of citrate-capped gold nanoparticles using UV induced nucleation, https://doi.org/10.1039/C6RA27173A, https://creativecommons.org/licenses/by/3.0/legalcode) [71].

All the above systems operated under Taylor flow (i. e. the equivalent droplet diameter was larger than the microchannel diameter). Lee et al. employed a flow-focusing microfluidic device (orifice $W \times H$: 50 µm × 110 µm) to generate microdroplets forming an emulsion (Figure 4.22). They used a silicone emulsifier (Abil-Em90) to prevent the coalescence of the microdroplets. The microdroplets contained a *N*-isopropylacrylamide (NIPAM) matrix, and when the NIPAM was polymerized it created a permeable membrane to isolate the inner compounds from the carrier solution. Thus, each droplet could function as an individual artificial cellular bioreactor to synthesize NPs by precursor solutions diffusing into the droplet. Au NPs with size 5–40 nm were obtained when different precursor concentrations (5–50 mM) were used [206].

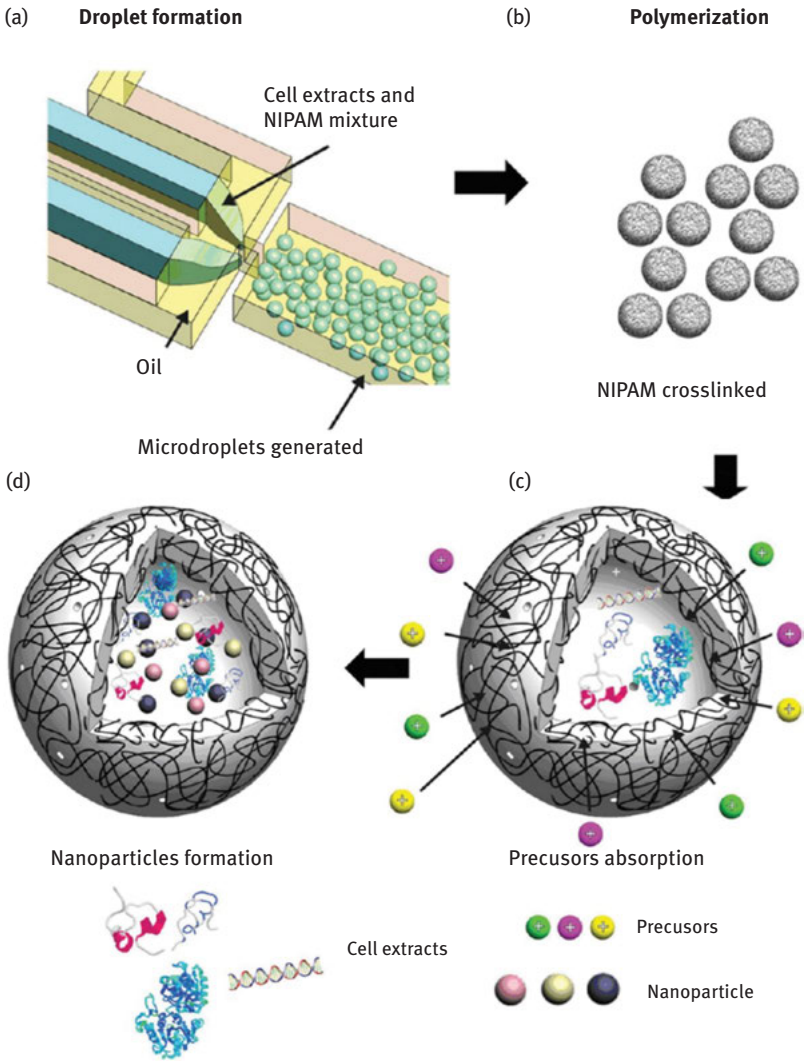

Figure 4.22: Schematic of microdroplet generation with the mixture of cell extracts and NIPAM monomer in a microfluidic device for nanoparticle synthesis (reprinted with permission from Ref. [207]. Copyright 2012, American Chemical Society).

Gu et al. proposed a novel method to dose the reducing agent ascorbic acid in the form of miniemulsion (continuous phase) into microfluidic droplets of gold precursor (dispersed phase). Transport of ascorbic acid from the miniemulsion nanodroplets into the microdroplets was achieved via electrocoalescence, induced by an applied alternating electrical field (Figure 4.23) [207]. The electrical field was applied between two parallel electrodes placed outside the FEP tube reactor (0.76 mm I.D.) without

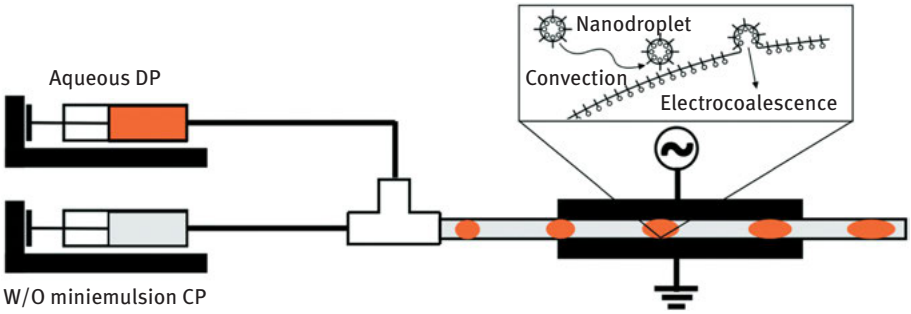

Figure 4.23: Experimental setup for dosing ascorbic acid from nanodroplets by electrocoalescence under high strength electrical field to synthesize Au NPs (adapted from Ref. [208]. with permission of The Royal Society of Chemistry, https://doi.org/10.1039/C8LC00114F).

any physical contact with the reactants and controlled the rate of addition of the reducing agent nanodroplets to the gold precursor microdroplets. PVP-capped Au NPs were produced with size tailored from 44.6 ± 12.6 nm to 81.2 ± 25.5 nm by the strength of the electrical field from 11,400 to 4300 V/cm.

4.3.2.2 Millifluidic reactors

Millifluidic slug flow reactors are less common due to difficulties in attaining stable slug flow in larger channels. Furthermore, as the size of the tube, and hence of the droplet, increases, mixing by internal recirculation within the droplet becomes less efficient. For this reason synthesis of NPs in millifluidic reactors has received less attention. Zhang et al. demonstrated a millidroplet reactor which could produce droplets with a volume of 0.25 ml inside a PTFE tube of I.D. 5.8 mm (Figure 4.24a) [208]. Co-axial flow with reversed flow direction of two streams was used to obtain better mixing in mixer T1 (Figure 4.24b). The well-mixed reagents were subsequently merged with silicon oil and formed a co-axial jet instead of droplets in the channel in mixer T2 and the exiting PTFE tube (I.D. = 1.58 mm). The jet was stabilized due to the high flow rate of the silicone oil stream, but when it entered the PTFE tube (I.D. = 5.8 mm) the flow rate for the silicone oil suddenly dropped, resulting in ml-sized droplets together with small, satellite droplets (Figure 4.24e). The satellite droplets merged quickly with the adjacent large droplets before they entered the reaction zone. With this setup, 10–30 nm spherical cetyltrimethylammonium chloride-capped Au NPs were produced by seeded growth with ascorbic acid, as well as Au cubes with 50 nm in edge length. The productivity of this system was in the 1–10 g/h range. The PTFE tube size of 5.8 mm appeared to be the largest size that could be used when silicone oil was employed as carrier phase. When tubes with larger diameter were used, it became difficult to generate stable droplets [53].

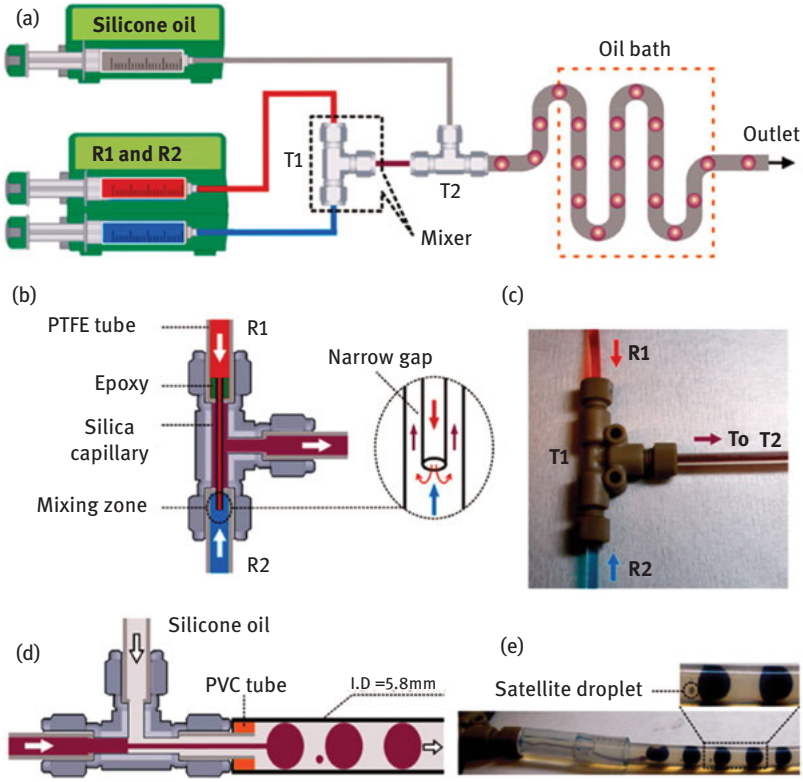

Figure 4.24: (a) Schematic illustration of the millilitre-sized droplet reactor used for the synthesis of Au NPs by ascorbic acid. (b) Schematic illustration of the flow mixer (T1) with three PTFE tubes connected to the T-junction and one silica tube fixed in the centre of the top PTFE tube. (c) Photograph of mixing demo based on the design of (b) with red and blue dye. (d) Schematic illustration of the design for droplet generating (T2). (e) Photograph of 0.25 ml droplets and 0.5 µl satellite droplets in the PTFE tube with an I.D. of 5.8 mm (reprinted with permission from Ref. [208]. Copyright 2014, American Chemical Society).

4.4 Guidelines for the design of continuous nanoparticle processes

4.4.1 A general overview of nanoparticle synthesis process development

The most important consideration for designing any Au NP synthesis process (batch or continuous flow) is the desired end use of the Au NPs. Since the properties of Au NPs vary depending on their size and shape, and also on their conjugated functionality, it is important to establish exactly what properties are required before starting any design process. There is no synthesis process that fits all needs. Many different synthesis processes produce Au NPs which are pre-functionalized with a specific

ligand which cannot be easily removed or exchanged and thus are only suitable in cases where the ligand has no impact on the application, or is the exact ligand required for said application. Similarly, some processes utilize toxic reagents which, though they might not be present in the final product, may make them unsuitable for pharmaceutical applications. Thus, the particular application will provide targets for size (or size range), polydispersity, choice of stabilization agents and throughput. The choice of stabilization agents affects hydrophobicity/philicity, subsequent functionalization, as well as long-term stability and storage of the particular nanoparticle formulation. It is important to note that if the conversion of the precursor is not complete during the synthesis, unreacted precursor will lead to nanoparticle growth/aggregation during storage.

Typically, there is more than one way to achieve the desired outcome. For example 7 nm particles functionalized with an amine can be achieved in a variety of ways. The Turkevich method has been shown to produce particles as small as 6 nm [71]. Such particles can be synthesized and consequently functionalized with other capping agents, such as thiol, cysteine or short proteins. Alternatively oleylamine-based synthesis can also achieve 7 nm Au NPs with very tight size control which can also subsequently be functionalized [209]. At the start of the design process it is important to establish as many suitable synthesis routes as possible, since one or more of these could later become discounted due to further complications downstream.

Once a suitable process (or processes) has been chosen there are several key design considerations which should be taken into account when trying to transfer an Au NP synthesis process into flow. Without being exhaustive, Figure 4.25 illustrates some of the considerations and challenges which can be encountered when developing an Au NP synthesis process, along with corresponding tools for addressing them. Some of the tools are chemistry-based, while others are engineering-based. Thus, a multidisciplinary approach will have more chances for developing an optimized process. Due to the relatively low annual production rates required and the sensitivity of most Au NP synthesis techniques, this schematic focuses on the design aspects which would be addressed for developing micro or millifluidic reactor systems.

As illustrated by Figure 4.25, there are relatively few design considerations to be made when developing a batch process, though their complexity should not be underestimated. In a typical batch process the chosen synthesis route is the greatest factor in the design, since this predetermines the size of the particles, their polydispersity and their functionality or ability to be functionalized. These properties can be manipulated by studying the kinetics of the system (as discussed earlier), where a design-of-experiments approach can also provide additional guidance. Varying the temperature, pH or chemical composition of a reaction mixture can be used to fine tune the process, but ultimately does not change the physical design of a batch reactor. Small batch systems, such as lab scale synthesis in a round bottom flask,

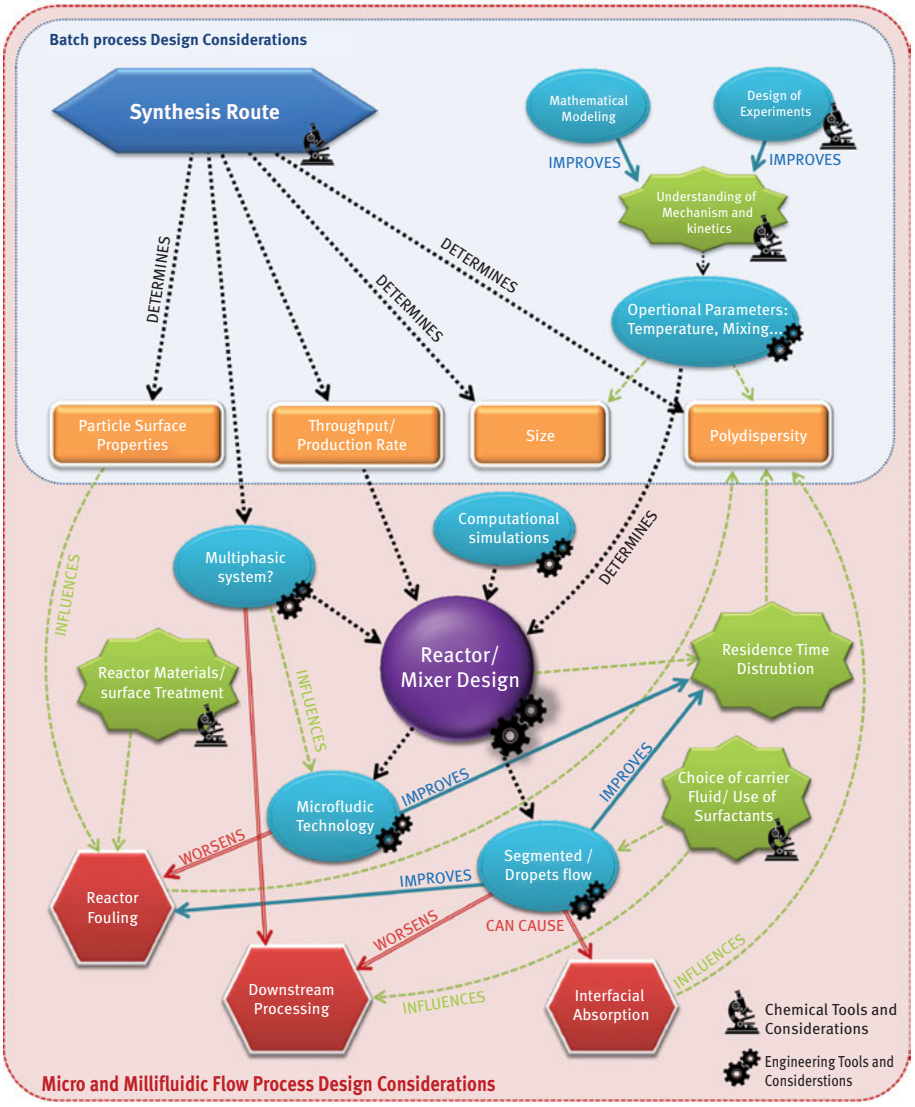

Figure 4.25: Key considerations for the development of a nanoparticle synthesis process in batch and flow systems "Chemical tools" indicate chemistry-based approaches for addressing the corresponding consideration, while "Engineering tools" indicate engineering-based approaches.

offer moderate reactor surface area to volume ratios (SA:Vs); this needs to be considered when synthesizing particles, since any surface or interface can act as a nucleation zone or potentially provide surfaces for fouling. This is less critical in larger vessels used for process scale-up, though other problems can arise, such as inefficient mixing/heating.

When the mixing efficiency of the reaction mixture plays an important role in product quality, batch reactors may be unsuitable. In cases where a reaction is very rapid (in the order of milliseconds), then it becomes crucial that the mixing time is even faster (or very well controlled), lest product quality suffers due to the formation of polydisperse particles. In this case the size of the reactor would be limited, since mixing efficiency decreases as reactor size increases. In addition to improving mixing as extensively demonstrated earlier, another way to control the process is slowing down the kinetics of the synthesis. A deeper understanding of the reaction kinetics can thus aid in identifying conditions for slowing down the synthesis, so that mixing speed is not the rate controlling step. By, for example, manipulating the pH of a system, the initial rate of reaction can be slowed and mixing can be allowed to complete before the reaction starts.

4.4.2 Challenges and solutions of micro/millifluidic processes

In contrast to batch process design, the scope of design considerations for developing a continuous flow process is much broader. In addition to all of the batch process design considerations, such as the fundamental reaction kinetics, understanding the physico-mechanical aspects of the reactors also becomes imperative. Unlike many chemical synthesis processes that only benefit from the improved RTD, mixing efficiency, heat transfer and control afforded by milli- and microfluidic devices, the synthesis of *particles* in flow systems is much more complex due to the potential for reactor surface interactions. This is due to the fact that surface area to volume ratio increases quickly in milli- and microfluidic devices. A batch reactor comprising of a 1 litre round bottom flask, for example, has a SA:V of approximately 0.5 cm^{-1}. This is much lower when compared to a 1 cm I.D. tube of the same volume which has a SA:V of 4 cm^{-1}, or a 0.5 mm I.D. capillary with a SA:V of 80 cm^{-1}. In addition to a vastly different SA:V, the materials employed also typically have drastically different physicochemical properties. Since a 1 litre reactor made from a 1 cm I.D. tube would have to be over 12 m long, the use of glass tubing becomes prohibitive and is thus typically substituted for etched glass chips with much lower volumes, or flexible plastic tubing. This means that the surface roughness and the surface chemistry of the reactors are not directly comparable with typical batch reactor systems and can have very different interactions. Altogether this may lead to fouling on the reactor walls.

4.4.2.1 Reactor design – residence time distribution

Control over the PSD is a key point for gold NPs synthesis, as many applications demand very reproducible and narrow size distributions, as discussed earlier. Recalling Figure 4.25, flow-synthesized particle characteristics are strongly affected by the RTD of the reactor. To explain what this distribution represents and why it

affects NPs synthesis in flow rectors, we first need to have a brief introduction to reactor design.

A general approach to tackle reactor design is to solve the mass, momentum and energy balance equations. If all the input data (flow conditions at the inlet, temperature and composition of the feed stream, etc.) and the reaction rate laws are known, this design approach is possible. Because the equations are coupled and complex to solve, they need to be integrated numerically by means of a computational fluid dynamics (CFD) code. CFD offers the advantage to reduce to the minimum the amount of assumptions required by the model. Its major drawback, however, is the relatively high computational cost of the simulations. It should be borne in mind that the reactor design procedure aims to provide an efficient relation between the input and output of the reactor that permits reducing the parameter space in which the designer must operate and determining the optimal conditions at which to operate the reactor. For this analysis – which involves scanning over a broad range of conditions – CFD models are not well suited. The appropriate models should be able to describe the reactor performance, with reasonable accuracy, at much less computational cost. To achieve this, one usually favours simpler models, based on a larger number of simplifying assumptions, that are fast to solve numerically and able to provide the information of interest to the accuracy required.

A modelling approach frequently employed consists of determining the contacting patterns in the reactor first and then use them to evaluate the reactor performance. The contacting patterns can be determined either by solving for the fluid dynamics in *absence of reaction* or by assuming the fluid dynamic behaviour so that the momentum balance equation does not need to be solved, or by experimentally analysing the behaviour of inert tracers in the reactor [210, 211]. Quantitatively, the contacting patterns are expressed by means of the RTD function [66]. Denoted by $E(t)$, this is defined so that $E(t)\mathrm{d}t$ yields the fraction of fluid that spends in the reactor a time in the range $\mathrm{d}t$ around the value t. Therefore, the RTD is a probability density function that describes the amount of time spent in the reactor by each fluid element (infinitesimally small macroscopically, but containing a statistically significant number of molecules).

One can imagine each one of these fluid elements as a batch reactor characterized by a certain reaction time t. The "weight" of the contribution of each fluid element to the overall reactor output is given by the RTD, which indicates how many fluid elements are characterized by any given residence time t. For continuous reactors synthesizing NPs, one is usually interested not only in the reactor conversion (as in "conventional" reactors), but also in the PSD. Denoted by $n(v)$, the PSD is defined so that $n(v)\mathrm{d}v$ yields the number of particles with volume in the range $\mathrm{d}v$ around v. If we know the time evolution of the PSD for a hypothetical batch reactor (even though we have pointed out how complex this is earlier), then the PSD at the outlet of a continuous flow reactor $\bar{n}(v)$ is given by:

$$\bar{n}(v) = \int_0^{+\infty} n(v,t)E(t)\mathrm{d}t.$$

This equation reveals the key role that the RTD plays in determining the characteristics of the NPs synthesized in a flow reactor. The width of the RTD makes the PSD of the continuous flow reactor differ from that of the batch (or of the plug flow) reactor. In particular, the "wider" the RTD, the "wider" the PSD. Hence, effort has to be put in "narrowing" the RTD of these reactors [43, 212–214]. It has been recently shown how the RTD-based approach can be employed to predict the outcome of flow reactors synthesizing NPs, taking into account different contacting patterns as well as the different diffusivities of precursors and NPs [215]. In this work, the PSD was determined for a single-phase (laminar) microreactor and a segmented flow microreactor as these reactors represent the most commonly encountered continuous reactors employed, as discussed earlier. While segmented flow reactors led to narrow PSDs due to their narrow RTD, single-phase laminar reactors characterized by a wider RTD, led to wider PSDs.

The RTD approach is no longer valid when mixing time significantly affects the synthesis product. In this case, PBEs have to be implemented within CFD codes to solve for the evolution of the PSD. This approach has been used by Marchisio and coworkers [216] to model a confined impinging jet reactor synthesizing barium sulphate NPs via a precipitation reaction. In this system, mixing and reaction have the same timescale, and so the RTD approach would not have been suitable.

4.4.2.2 Reactor fouling/interfacial absorption

Fouling (either due to fully formed particles depositing on the reactor walls or from reactants reacting and plating the walls) often creates complications in milli- and microfluidic flow systems used for synthesizing particles. Not only does fouling lead to a loss of material, and therefore a lower product yield, but it can also create secondary heterogeneous nucleation sites and "particle incubation zones". Since the rate of nucleation on the tubing walls would be inherently different than that in the bulk of the solution, this can lead to increased polydispersity in the product. Similarly, if particles foul or get temporarily entrapped on or in the surface of the material where the concentration of unreacted Au NP precursors is still high, they can continue to grow to much larger sizes, and often take on unusual shapes. The slow build-up of fouling also leads to a gradual change in the reactor's physical properties during use (from hydrophobic to hydrophilic for example). This can lead to a variable product, since the yield and polydispersity change as fouling increases and can eventually even block the flow through the reactors. This is especially evident when using synthesis techniques where the Au NPs are charge stabilized, such as the classical citrate reduction method. As illustrated in Figure 4.26, a purple-gold

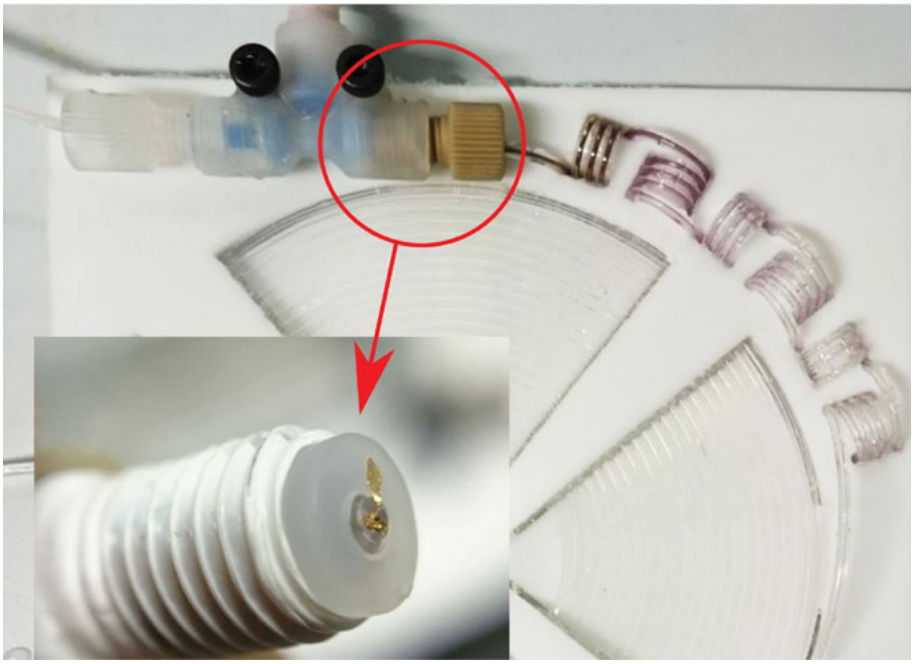

Figure 4.26: Typical level of fouling observed when classical citrate reduction was employed in a microfluidic reactor (0.5 mm I.D. FEP tubing) with flows of 0.2 ml/min each of a 1 mM $HAuCl_4$ solution and a 5 mM trisodium citrate solution mixed with a T-mixer at 90 °C. Blockage (inset) observed after approximately 8 h continuous operation.

fouling was often evident immediately after the reagents ($HAuCl_4$ and $Na_3C_6H_5O_7$) were mixed. During prolonged operation, the level of fouling could be so high as to form sheets of gold leaf inside the tubing which eventually led to the formation of blockages (Figure 4.26 inset).

In order to counteract fouling various techniques can be employed. Since a high SA:V is difficult to overcome without sacrificing on efficient heat and mass transfer, as well as the residence time (or RTD), physicochemical steps are generally taken to discourage fouling, and some of them have been detailed earlier. These include carefully considering the choice of tubing material (the use of high density plastics, or plastics with a lower porosity), chemically treating tubing to change the hydrophobicity [217] and surface charge, or the use of segmented flow to prevent contact between the reaction medium and the tubing wall. However, it is important to note that each step taken to prevent fouling can lead to further complications of their own. A chemical surface treatment can wear off over time, contaminating the product and causing variable conditions inside the reactor. The use of immiscible segmenting fluids can cause interfacial absorption [218] and can also increase the complexity of downstream processing, since the carrier fluid would then have to be separated from

the product. Figure 4.27a illustrates how extensive interfacial absorption can be. In this case toluene was compared with dodecane to create segmented flows for a classical citrate reduction Au NP synthesis method. Both fluids prevented fouling within the reactor; however, in the case of toluene nearly all of the synthesized particles were lost due to interfacial absorption.

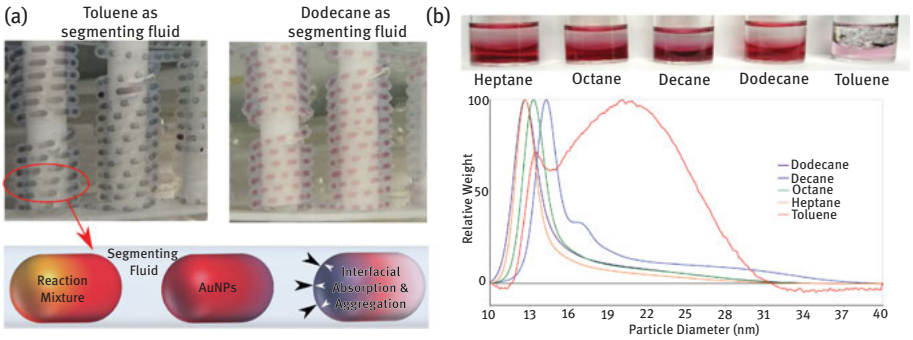

Figure 4.27: The effect of different segmenting fluids on the interfacial absorption of Au NPs during classical citrate reduction synthesis (a reaction mixture consisting of 0.5 mM $HAuCl_4$, 5 mM trisodium citrate and 1 mM citric acid prepared in-line at room temperature) segmented with the chosen segmenting fluid using a T-mixer before entering a hot (90 °C) millifluidic reactor (2.1 mm I.D. FEP tubing); (A) schematic and photos illustrating the occurrence of interfacial absorption, and (B) effect of interfacial absorption on the PSD of the remaining Au NPs depending on the segmenting fluid chosen (measured by differential centrifugal sedimentation).

In addition to leading to a loss of material, the occurrence of interfacial absorption can also affect the size and size distribution of the particles that remain. Figure 4.27b shows the PSDs achieved when the same reaction mixture was segmented with five different segmenting fluids, namely heptane, octane, decane, dodecane and toluene. In addition to the loss of material observed through the appearance of a dark film of aggregates at the interface between solutions (with toluene being by far the worst), the size and size distributions varied in each case. This suggests that similarly to fouling on the reactor wall, the occurrence of interfacial absorption also leads to heterogeneous nucleation sites or "particle incubation zones". In order to reduce this effect it is clear that a good understanding of the interactions between fluids is required, but also that a certain degree of investigation is needed to determine the best segmenting fluid to use. In Figure 4.27b for example, there does not appear to be a distinct trend between the length of the alkane used (and consequently the density, viscosity, miscibility or interfacial surface tension) and its effect on particle size, but it is evident that both heptane and dodecane performed best.

Ultimately fouling, or the secondary complications arising from attempts to mitigate fouling, might not be overcome to a satisfactory standard (if, for example, the added downstream processing becomes cost prohibitive). In these cases it is worth

reconsidering which synthesis routes are available, which will ultimately produce the same product. For example, Au NPs conjugated with thiol-based molecules have a much lower prevalence to foul. A route which employs these ligands during synthesis will not present as much of a fouling problem, so, if what is needed is amine functionalized Au NPs, it might be best to use a process that employs an amine thiol.

4.4.2.3 Multiphasic reaction systems

The use of multiphasic reaction systems must be carefully considered when designing a continuous flow process. This is not only due to the added difficulties involved in in-flow phase separation, but also due to the different interfacial surface areas achieved in batch and flow systems (analogous to the difference in SA:V between batch and flow systems). In multiphase reaction systems (where reactants are separated by a phase boundary), maintaining a constant size of the interface is paramount in order to ensure that the product produced is of good and reproducible quality. This is due to the fact that the interfacial surface area limits the rate at which reactants and products can be transferred between phases.

In batch systems, the interface between two phases is dynamic with both solutions free to circulate throughout the reactor and disperse into each other through the formation of droplets under agitation. Since the phases are not isolated (droplets can subsequently coalesce and re-join the bulk of the solutions) a chaotic and poorly regulated interface is present. The formation of additional phases (such as the evolution of gas) does not interfere, since gas bubbles are rapidly removed from the system. In contrast, when using a milli or microfluidic reactor system, each droplet is spatially isolated from the next. Thus each droplet has its own interface and ensuring that each droplet has the same interfacial surface area is necessary. Thus, systems like this have to be well ordered. In order to achieve the same rate of phase transfer, the size of each droplet has to be identical every time the experiment is run. This can be difficult to achieve, especially in cases where gas evolution also takes place.

A good example to illustrate the potential complications of using multiphasic reaction systems in a continuous flow process is the technique for synthesizing thiol capped Au NPs proposed by Brust et al. [157]. In the classical Brust-Schiffrin method, a prepared Au(x) and dodecanethiol in toluene solution (where x denotes the mixture of Au(I) and Au(III) resulting from the partial and incomplete reduction of Au(III) to Au(I) by dodecanethiol), is continuously mixed with an aqueous $NaBH_4$ solution to facilitate the reduction of the Au(x) to Au(0) forming dodecanethiol capped Au NPs. The reduction of Au(x) by $NaBH_4$ results in the rapid evolution of hydrogen gas.

Since the interface between the toluene and the water phases plays an important role during reduction, either as the site of the reaction or as the medium through which phase transfer of $NaBH_4$ occurs, it is important to maximize the size of this interface in flow. The most obvious choice is thus to employ droplet flow with small droplets of an Au(x) solution dispersed in an aqueous $NaBH_4$ solution as

this ensures the greatest possible interfacial surface area. However, as illustrated by Figure 4.28, complications can arise in this case due to the evolution of hydrogen gas.

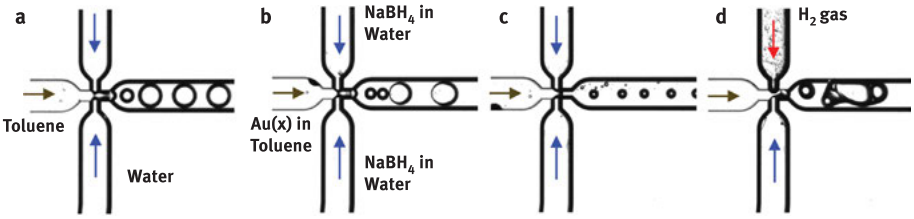

Figure 4.28: Multiphasic reaction system in a microfluidic droplet chip (3200130, Dolomite); (a) toluene (50 µl/min) as dispersed/droplet phase and water (210 µl/min) as continuous phase, (b–d) a 11.25 mM Au(*x*), 10.5 mM dodecanthiol and 50 mM tetraoctylammonium bromide in toluene solution as the dispersed phase (50 µl/min) and 30 mM $NaBH_4$ aqueous solution as continuous phase (210 µl/min).

As can be seen in Figure 4.28a, when pure toluene and water were used, stable droplet flow was achieved with uniform sized toluene droplets which would result in very high interfacial surface areas for the transfer of $NaBH_4$ into toluene. However, when the reactant solutions were used, highly variable and uncontrolled flow was achieved due to the rapid evolution of hydrogen gas in the aqueous $NaBH_4$ stream. This not only resulted in inconsistent droplet sizes (Figure 4.28b and Figure 4.28c), but also in a complex three-phase flow where the toluene and water phases did not make contact (Figure 4.28d). The end result was that the droplet flow was unstable causing the coalescence of the toluene droplets to form segmented or slug flow. These segments were uneven in size, not uniformly distributed, and often separated by H_2 gas segments. Figure 4.29 shows the particles produced in the batch and flow processes as analysed by TEM. The particles produced in the batch experiment were very similar to the particles produced in the classical Brust-Schiffrin method with an average particle size of 2.3 ± 0.4 nm. In contrast, the particles produced in segmented flow were more polydispersed, with a significant number of larger Au NPs (approximately 5 nm) produced as well. These results are likely a result of H_2 gas formation. As illustrated in Figure 4.29b, the evolution of gas in a segmented flow system results in a reduction of the interfacial surface area between the aqueous solution and toluene, since the gas bubbles form segments of their own which block the interaction between the phases. In addition, the evolution of gas increases the overall flow rate and therefore reduces the actual residence time in the reactor. Conversely, in a batch system (Figure 4.29a), the evolution of gas bubbles enhances mixing and recirculation of material in both phases. Since the gas is free to escape there is also no build-up at the interface between the water and toluene phases, so no “blocking” effect is achieved. This results in smaller and less polydisperse particles.

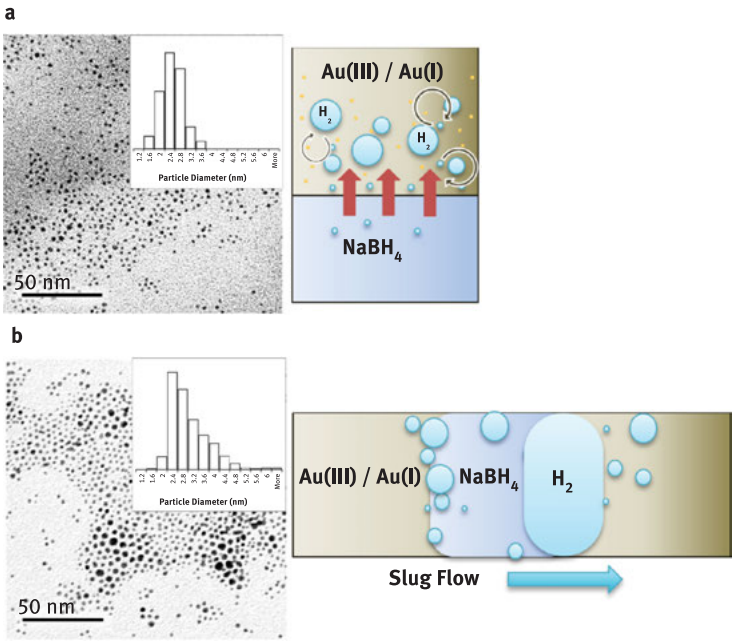

Figure 4.29: Particle size distributions and schematic of flow patterns obtained in; (a) batch and (b) continuous flow "Brust-Schiffrin" synthesis of dodecanethiol capped Au NPs. In both cases, 11.25 mM Au(*x*), 10.5 mM dodecanthiol and 50 mM tetraoctylammonium bromide in toluene solution were employed with a 120 mM $NaBH_4$ and 725 mM NaOH aqueous solution. The batch experiment utilized 2 ml of each solution in flask agitated by magnetic stirrer for 1 h. The continuous flow setup utilized a T-mixer to create segmented flow through a length of FEP tubing (5 m long, 0.5 mm I.D., 1.0 ml volume) with both solutions flowing at approximately 0.5 ml/h resulting in a 1 h residence time. Size distributions were determined by TEM.

A potential solution to this problem is to prevent the evolution of hydrogen gas from the $NaBH_4$ by either using much lower concentrations (so that the H_2 formed remains dissolved in the water), or to use higher pH solution to buffer the release of H^+ from $NaBH_4$ and thus prevent the formation of H_2 altogether. These types of changes could however have knock-on effects on the chemistry of the Au NP synthesis reactions. Changing the concentrations of reactants can change the kinetics and mechanisms involved in particle formation, resulting in Au NPs of different sizes or in the formation of by-products. Altering the pH can also change the species of the reactants present which can in turn alter their reactivity.

4.4.2.4 Downstream processing

Whenever continuous flow reactor systems are used, continuous downstream processing needs to be considered. The benefits attained by continuous manufacturing processes could be lessened if downstream processing is conducted in a batch wise

fashion. For example, there is little gain from continuously synthesizing Au NPs, if one then has to wait and collect a litre at a time to purify and wash the products in batches. If synthesis is conducted in flow, then downstream processing (purification, precipitation or further functionalization, etc.) should also be conducted in flow.

One of the principle concerns in continuous flow downstream processing involved in Au NP production is phase separation. Using segmented flow to control RTD, prevent fouling or due to the fact that the reaction system is multiphasic, creates the need to subsequently separate the phases. In a batch manufacturing process this is simple, since different phases will naturally separate in the reactor due to gravity. Gas bubbles will dissipate and oils will self-separate and fractionate based on their density, allowing the Au NP phase to be siphoned off. However, in a flow system phase separation is more complex and typically requires additional equipment such as a membrane separator.

Figure 4.30 shows a continuous flow membrane separator which can perform in-line phase separation of a segmented flow stream [219]. A PTFE membrane is used to separate a hydrophilic phase from a hydrophobic phase which readily wets the PTFE membrane. When a membrane-based continuous flow phase separator is employed, it is important to ensure that the pressure difference across the membrane is tightly

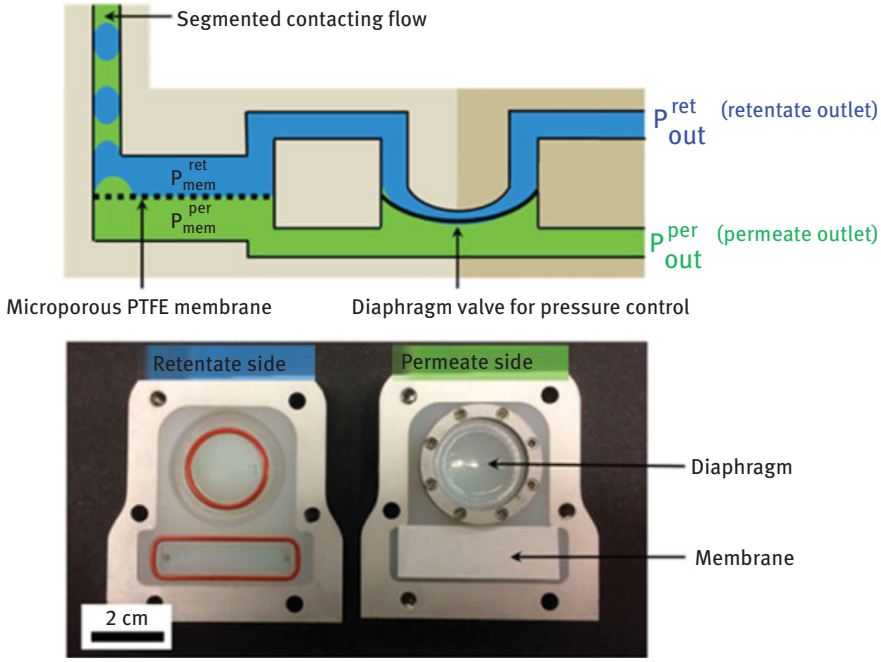

Figure 4.30: Schematic of operation and pictures of a disassembled membrane-based separator integrated with a self-tuning pressure control element (reprinted with permission from Ref. [220]. Copyright 2017, American Chemical Society).

controlled to avoid breakthrough, where both phases cross the membrane and separation is not achieved. This typically requires the use of back pressure regulators to modulate the outlet pressure of the two streams exiting the membrane separator, which not only increase the complexity of the system, but can greatly increase the cost of operation. In the separator shown in Figure 4.30 an integrated diaphragm is used to modulate the pressure between the two outlet streams and ensure that the pressure drop across the membrane is kept stable.

The introduction of such systems can result in the introduction of new problems. Fouling is a key concern whenever additional materials are introduced to a flow system (especially high surface area materials such as a membrane). We must also consider what would happen to any particles that are trapped at the phase interface due to interfacial absorption. Either these particles are forced through the membrane and leave in the permeate, are retained in the retentate, or become lodged in the membrane itself. Each of these scenarios can have significant implications for the continuous production process. In a continuous flow system it might be apt to employ several redundancies (multiple interchangeable membrane separators for example) which can allow for routine maintenance and downtime to mitigate potential problems.

Another major downstream processing operation is the continuous purification of Au NPs in flow. Many synthesis routes use one or more reactants or functionalizing agents in excess. Prior to the use of Au NPs from such synthesis techniques, the Au NP mixture has to be purified to remove these superfluous reagents. This typically involves a complex multistage process to remove the Au NPs from solution and then to repeatedly wash the particles. For example, in the classical Brust-Schiffrin method the synthesized thiolate Au NPs have to be precipitated and washed prior to use. The precipitation process involves the concentration of the Au NP in toluene solution by evaporation of toluene (an energy intensive process), the subsequent addition of a large volume of ethanol to increase the polarity of the solvent, and refrigeration (typically −18 °C for 4 h). Following precipitation the particles are removed from the solution via filtration and redispersed in toluene. The overall process is time consuming and energy intensive. It is also difficult to adapt to flow, since the process of concentrating, diluting with ethanol, cooling for 4 h, and filtration would involve many different unit operations. Thus a new approach is required.

Figure 4.31 illustrates a procedure for the in-line purification of thiolate Au NPs using continuous diafiltration [220]. In this case, slightly different water-soluble thiolate Au NPs were purified. The crude Au NP mixture was mixed with fresh solvent prior to passing through a dialysis membrane. Since the Au NPs were too large to pass through the membrane they exited the membrane in the retentate with a small amount of the solvent. The vast majority of the impurities were removed with the majority of the solvent in the permeate. Though not as effective a purification technique as precipitation and washing (where all impurities are considered

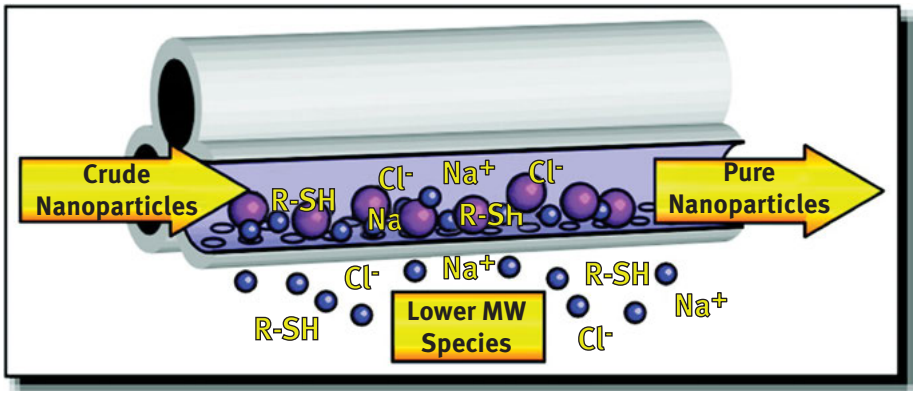

Figure 4.31: Schematic of continuous diafiltration of water-soluble thiol-stabilized 3-nm gold nanoparticles. Small molecule impurities and small gold nanoparticles (blue) are eluted in the permeate, while the larger gold nanoparticles (purple) are retained (reprinted with permission from Ref. [221]. Copyright 2006, American Chemical Society).

removed) this technique is much less energy intensive and less time consuming, since it can be performed in-line with the original reactor system. It thus provides a good compromise to the batch purification process without the costs and complexities associated with adapting the native "Brust-Schiffrin" purification process to flow. Such in-line tangential flow filtration (TFF) integrated with a millifluidic reactor was demonstrated by Lohse et al. for the removal of CTAB and by-products from the crude reaction product of gold nanorods synthesis and thiol exchange on gold nanorods [181]. TFF can potentially reduce product losses due to aggregation, because the Au NPs are not forced into close physical contact as for example during centrifugation. This type of approach relies on well stabilized Au NPs. Such high surface area membranes might be susceptible to fouling from particles which are not well stabilized, such as simple citrate charge stabilized particles. The message behind continuous flow purification, downstream processing, and indeed any flow process relating to the manufacture of Au NPs, is that compromise will be necessary and complications are likely. It is important to have a wide ranging arsenal for dealing with these problems and to be highly flexible in one's approach. If for example the Au NPs synthesized with one particular synthesis route cannot be effectively purified in flow, then it may be prudent to pursue an alternative synthesis route altogether.

4.4.2.5 Summary of main design rules for continuous flow NP reactor design

The discussion above clearly reveals the complexity of the design of continuous flow reactors for the synthesis of NPs. A large number of aspects, most of which are closely related, need to be considered, while all the necessary information (such as kinetics of synthesis processes) to make fully informed decisions, are not always available.

Here, we present a brief summary of the main design rules that we suggest should be followed when undertaking the design of continuous flow reactors for gold nanoparticle synthesis.

1. Specify the desired end use of the Au NPs, and identify the desired Au NP properties (size, polydispersity, shape, functionality, etc.) and final process targets (throughput, purity).
2. Identify a range of suitable synthesis routes and consider each one individually.
3. Gather kinetic data for the reactions (and any other relevant process) involved, if possible. Estimate their characteristic times and assess how critical are the heat and mass transfer rates.
4. Depending on the desired throughput and on how fast the relevant kinetics are, decide whether to use a milli- or a microreactor. For larger throughputs and syntheses involving slower reactions, millireactors should be more suitable.
5. Assess the implications of mixing and RTD on PSD, which are usually more severe for larger diameter devices and single-phase reactors.
6. If fouling presents a problem, multiphase reactors (in which the flow is segmented) may be more suitable. Consider, however, the implications in terms of downstream processing and select carefully the segmenting fluid to minimize interfacial absorption.
7. If a single-phase reactor is preferable, select a channel material that prevents or reduces fouling, treat the tube or manipulate the synthesis chemistry.
8. Design the reactor and select operating conditions that result to full consumption of precursor.
9. Select the operating conditions carefully. Low concentrations and appropriate pH can be used to reduce or prevent the formation of gas products.
10. Consider separation and purification procedures at the outset, as these may affect process viability.

We also recommend considering the schematic in Figure 4.25, which, in addition presenting the key considerations for the development of nanoparticle synthesis processes in batch and flow systems, highlights as well their multiple connections.

4.5 Critical safety considerations

While many of the materials employed for the syntheses of Au NPs described in this chapter are safe to use (e. g. sodium citrate or ascorbic acid), some of the chemicals are toxic and/or flammable, hence they should be carefully handled and the experimental conditions should be strictly controlled.

1. Read the Material Safety Data Sheet (MSDS) before using any chemicals. The hazardous chemicals (with labels like Explosive, Highly Flammable, Toxic, Harmful, Corrosive, Oxidizing or Irritant) should be strictly controlled and stored

under proper conditions. A spillage kit suitable for the types of chemicals being handled, as well as the correct type of personal protective equipment (PPE) must be used. If special first-aid facilities or equipment (e. g. extinguishing media) are required, then training is essential in their use. For environmental precautions, do not let chemicals enter drains. Store the chemicals in cool place. Keep containers tightly closed in a dry and well-ventilated place.

2. If using special experimental conditions (e. g. elevated temperature, high pressure, microwaves, lasers or radiation), suitable training is required. All the relevant equipment should be checked regularly to ensure their proper operation. Appropriate operating procedures are required for risk management.
3. Gold(III) chloride hydrate needs special attention, since it is corrosive to metals and to skin, and can cause serious eye damage and skin sensitization. For safe storage, note that gold(III) chloride hydrate is light sensitive and strongly hygroscopic.
4. Sodium borohydride, a widely used strong reducing agent, could emit flammable gases which may ignite spontaneously in contact with water. Thus, it should be handled under inert gas and protected from moisture. For cleaning up, do not flush with water. Keep in suitable, closed containers for disposal. For firefighting measures, the suitable extinguishing media is dry powder.
5. For the use of thiols, be aware that special hazards (sulphur oxides) might arise from the substance or mixture.
6. Aqua regia is commonly used to clean up the apparatuses used to synthesize Au NPs. It is acutely toxic if inhaled or ingested, corrosive to skin and eyes and extremely destructive to the tissue of the mucous membranes and upper respiratory tract. It should be kept and stored away from clothing/combustible materials. Appropriate PPE (lab coat, safety glasses, with side shields or splash goggles and gloves compatible with nitric and hydrochloric acid) should always be used. Handling of aqua regia must be done only inside a fume hood and with glassware. Mix the solution in a fume hood with the sash between you and the solution. Never add any organics to aqua regia solution, it could cause an explosion. When preparing aqua regia, always add nitric acid to hydrochloric acid, never vice versa. Never store aqua regia solutions, as it will oxidize over time to form toxic gases. Make only small, fresh batches of aqua regia for each use.
7. Where hazardous or flammable gases (e. g. CO, hydrogen) are intended to be used, gas alarms/monitors are required and cylinders must be stored in vented enclosures. Purge the reactor system with dry inert gas (e. g. helium or nitrogen) before the hazardous gas is introduced and when the system is switched off. Keep away from combustible materials, heat, hot surfaces, sparks, open flames and other ignition sources.

4.6 Conclusions and future perspective

If the predicted markets for Au NPs reach their full potential, their demand will increase significantly. Since their performance is critically affected by their properties (size, size distribution, composition, surface functionality), even small deviations can render them unsuitable for the target application. Obtaining Au NPs with consistent properties with robust manufacturing processes will be required. Currently manufacturing of Au NPs is based on batch processes, which are similar to the ones used for their lab synthesis. Batch-to-batch variability however can be an issue, particularly as the scale increases, due to the inherent limitations of batch processes in terms of mass/heat transfer, hydrodynamics and reaction time control.

Microreactors and millireactors can solve some of the challenges faced to achieve high quality/quantity products. This has been demonstrated by various studies, using for example controlled or fast mixing devices, segmented flow systems, dynamic reactor operation. Such reactors can overcome issues of reproducibility, scalability and size control. They can be complex, but others, mainly millifluidic reactors, are more user-friendly. However, even though flow systems address some limitations of current batch reactor technology, they may introduce other challenges that need to be resolved before they become mainstream synthesis technology. Some of these originate from the fact that even though high surface-to-volume ratios of micro- and millifluidic reactors is advantageous in terms of mass and heat transfer, it may introduce reactor fouling.

In this chapter, we attempted to give an overview of the various challenges that can be encountered in the development of continuous Au NP synthesis and gave guidelines of how they can be addressed. Our suggestions are by no means complete. The area is at an early stage of maturity and will benefit by additional research to better understand the various physicochemical phenomena involved in the synthesis, as well as comprehensively analyse reactor performance by modelling tools. By approaching the process design in a multidisciplinary fashion, new tools and innovative solutions can be devised. This is particularly so, because nanoparticle synthesis is complex, requiring knowledge of synthetic/physical/analytical chemistry, physics, particle technology and chemical engineering. Such multidisciplinary research can expand the range of solutions available. For example, the fouling issue can be tackled from an engineering perspective through segmented flow or from a chemistry perspective by changing the synthesis chemistry reactor wall properties.

It is worth mentioning that most studies on nanoparticle synthesis in microreactors translated batch protocols to a flow process. This approach though overlooks the unique advantages offered by microreactors, such as fast heating/cooling, high pressure operation, short reaction times, staged addition of reactants. Thus, there may be new opportunities, if the advantages offered by flow operation are considered from the beginning.

Contributions from reactor engineering, separation technology, process analytic and control, chemical/systems engineering will be vital for the development of robust, reliable, cost-effective manufacturing processes, with long operating times.

Traditional chemical engineering can play an important role here. Furthermore, a knowledge-based approach, relying on mechanistic and kinetic studies of reaction, nucleation and growth can lead to the development of robust well-designed processes. However, such a rigorous approach can be time consuming, so one must consider an appropriate balance between rigour and practicality. Design of experiments can play a role in this context and can aid in minimizing the effort invested in and maximizing information obtained from experiments.

As the scale of production increases, process yield and product purity become as important as size, shape, monodispersity. Efficient coupling of the synthesis with downstream processing and purification, as well as with analytical systems for in-line/online product characterization and process control will affect process economic viability. Lessons can be learned from the various microfluidic systems that have been used with *in situ* analysis, aiming to better understand the nanoparticle mechanism and kinetics. The emergence of advanced software, machine learning and the industry 4.0 framework will allow high level of process automation. Notwithstanding that, manufacturing routes will need to be carefully selected based not only on the scalability and production cost, but also on the particular properties required for the final application.

Acknowledgements: We would like to acknowledge funding for our research from EPSRC (grant EP/M015157/1) and European Union's Horizon 2020 research and innovation programme under the Marie Skłodowska-Curie grant agreement No. 721290. A special thanks to Prof. Peter Dobson and Prof. Ivan Parkin for their insightful feedback to this chapter and our work in general. He Huang acknowledges support from the program of China Scholarships. This publication reflects only the authors' view, exempting the Community from any liability.

References

[1] Daniel MC, Astruc D. Gold nanoparticles: assembly, supramolecular chemistry, quantum-size related properties and applications toward biology, catalysis and nanotechnology. Chem Rev. 2004;104:293–346.
[2] Barreto JA, O'Malley W, Kubeil M, Graham B, Stephan H, Spiccia L. Nanomaterials: applications in cancer imaging and therapy. Adv Mater. 2011;23:12.
[3] In: Rai M., Shegokar R., editor(s). Metal nanoparticles in pharma. Cham: Springer, 2017
[4] Thota S, Crans DC. Metal nanoparticles: synthesis and applications in pharmaceutical sciences. Weinheim: John Wiley & Sons, 2018
[5] Dykman L, Khlebtsov N. Gold nanoparticles in biomedical applications: recent advances and perspectives. Chem Soc Rev. 2012;41:2256–82.
[6] Yang X, Yang M, Pang B, Vara M, Xia Y. Gold nanomaterials at work in biomedicine. Chem Rev. 2015;115:10410–88.
[7] Dreaden EC, Alkilany AM, Huang X, Murphy CJ, El-Sayed MA. The golden age: gold nanoparticles for biomedicine. Chem Soc Rev. 2012;41:2740–79.
[8] Sardar R, Funston AM, Mulvaney P, Murray RW. Gold nanoparticles: past, present, and future. Langmuir. 2009;25:13840–51.

[9] Willets KA, Van Duyne RP. Localized surface plasmon resonance spectroscopy and sensing. Annu Rev Phys Chem. 2007;58:267–97.
[10] Wilson R. The use of gold nanoparticles in diagnostics and detection. Chem Soc Rev. 2008;37:2028–45.
[11] Lane LA, Qian X, Nie S. SERS nanoparticles in medicine: from label-free detection to spectroscopic tagging. Chem Rev. 2015;115:10489–529.
[12] Saha K, Agasti SS, Kim C, Li X, Rotello VM. Gold nanoparticles in chemical and biological sensing. Chem Rev. 2012;112:2739–79.
[13] Zhang Y, Chu W, Foroushani AD, Wang H, Li D, Liu J, et al. New gold nanostructures for sensor applications: a review. Materials. 2014;7:5169–201.
[14] Matias AS, Carlos FF, Pedrosa P, Fernandes AR, Baptista PV. Gold nanoparticles in molecular diagnostics and molecular therapeutics. In: Rai M., Shegokar R, editor(s). Metal nanoparticles in pharma. Cham: Springer, 2017:365–87.
[15] Zhou W, Gao X, Liu D, Chen X. Gold nanoparticles for in vitro diagnostics. Chem Rev. 2015;115:10575–636.
[16] Vs AP, Joseph P, Scg KD, Lakshmanan S, Kinoshita T, Muthusamy S. Colorimetric sensors for rapid detection of various analytes. Mater Sci Eng: C. 2017;78:1231–45.
[17] Singh J, Sharma S, Nara S. Evaluation of gold nanoparticle based lateral flow assays for diagnosis of enterobacteriaceae members in food and water. Food Chem. 2015;170:470–83.
[18] Bahadır EB, Sezgintürk MK. Lateral flow assays: principles, designs and labels. TrAC Trends Anal Chem. 2016;82:286–306.
[19] Quesada-González D, Merkoçi A. Nanoparticle-based lateral flow biosensors. Biosens Bioelectron. 2015;73:47–63.
[20] Cordeiro M, Ferreira Carlos F, Pedrosa P, Lopez A, Baptista PV. Gold nanoparticles for diagnostics: advances towards points of care. Diagnostics. 2016;6:43.
[21] Huang X, Jain PK, El-Sayed IH, El-Sayed MA. Gold nanoparticles: interesting optical properties and recent applications in cancer diagnostics and therapy. Nanomedicine. 2007;2:681–93.
[22] Kumar A, Zhang X, Liang X-J. Gold nanoparticles: emerging paradigm for targeted drug delivery system. Biotechnol Adv. 2013;31:593–606.
[23] Alkilany AM, Thompson LB, Boulos SP, Sisco PN, Murphy CJ. Gold nanorods: their potential for photothermal therapeutics and drug delivery, tempered by the complexity of their biological interactions. Adv Drug Deliv Rev. 2012;64:190–9.
[24] Abadeer NS, Murphy CJ. Recent progress in cancer thermal therapy using gold nanoparticles. J Phys Chem C. 2016;120:4691–716.
[25] Yao C, Zhang L, Wang J, He Y, Xin J, Wang S, et al. Gold nanoparticle mediated phototherapy for cancer. J Nanomater. 2016;2016:Article ID 5497136
[26] Hwang S, Nam J, Jung S, Song J, Doh H, Kim S. Gold nanoparticle-mediated photothermal therapy: current status and future perspective. Nanomedicine. 2014;9:2003–22.
[27] Haume K, Rosa S, Grellet S, Śmiałek MA, Butterworth KT, Solov'yov AV, et al. Gold nanoparticles for cancer radiotherapy: a review. Cancer Nanotechnol. 2016;7:8.
[28] Her S, Jaffray DA, Allen C. Gold nanoparticles for applications in cancer radiotherapy: mechanisms and recent advancements. Adv Drug Deliv Rev. 2017;109:84–101.
[29] Corma A, Garcia H. Supported gold nanoparticles as catalysts for organic reactions. Chem Soc Rev. 2008;37:2096–126.
[30] Stratakis M, Garcia H. Catalysis by supported gold nanoparticles: beyond aerobic oxidative processes. Chem Rev. 2012;112:4469–506.
[31] Ciriminna R, Falletta E, Della Pina C, Teles JH, Pagliaro M. Industrial applications of gold catalysis. Angew Chem Int Ed. 2016;55:14210–7.

[32] Cebrián V, Martín-Saavedra F, Yagüe C, Arruebo M, Santamaría J, Vilaboa N. Size-dependent transfection efficiency of PEI-coated gold nanoparticles. Acta Biomater. 2011;7:3645–55.
[33] Chithrani BD, Ghazani AA, Chan WC. Determining the size and shape dependence of gold nanoparticle uptake into mammalian cells. Nano Lett. 2006;6:662–8.
[34] Leifert A, Pan-Bartnek Y, Simon U, Jahnen-Dechent W. Molecularly stabilised ultrasmall gold nanoparticles: synthesis, characterization and bioactivity. Nanoscale. 2013;5:6224–42.
[35] Dykman L, Khlebtsov N. Gold nanoparticles in biology and medicine: recent advances and prospects. Acta Nat. 2011;3:34–55
[36] Pan Y, Neuss S, Leifert A, Fischler M, Wen F, Simon U, et al. Size-dependent cytotoxicity of gold nanoparticles. Small. 2007;3:1941–9.
[37] Hvolbæk B, Janssens TV, Clausen BS, Falsig H, Christensen CH, Nørskov JK. Catalytic activity of Au nanoparticles. Nano Today. 2007;2:14–8.
[38] Hashmi ASK, Rudolph M. Gold catalysis in total synthesis. Chem Soc Rev. 2008;37:1766–75.
[39] Sebastian V, Arruebo M, Santamaria J. Reaction engineering strategies for the production of inorganic nanomaterials. Small. 2014;10:835–53.
[40] Valencia PM, Farokhzad OC, Karnik R, Langer R. Microfluidic technologies for accelerating the clinical translation of nanoparticles. Nat Nanotechnol. 2012;7:623.
[41] Krishna KS, Li Y, Li S, Kumar CS. Lab-on-a-chip synthesis of inorganic nanomaterials and quantum dots for biomedical applications. Adv Drug Deliv Rev. 2013;65:1470–95.
[42] Puigmartí-Luis J. Microfluidic platforms: a mainstream technology for the preparation of crystals. Chem Soc Rev. 2014;43:2253–71.
[43] Marre S, Jensen KF. Synthesis of micro and nanostructures in microfluidic systems. Chem Soc Rev. 2010;39:1183–202.
[44] Tsuzuki T. Commercial scale production of inorganic nanoparticles. Int J Nanotechnol. 2009;6:567–78.
[45] Taifur-Rahman M, Rebrov E. Microreactors for gold nanoparticles synthesis: from Faraday to flow. Processes. 2014;2:466.
[46] deMello AJ. Control and detection of chemical reactions in microfluidic systems. Nature. 2006;442:394–402.
[47] Nightingale AM, deMello JC. Segmented flow reactors for nanocrystal synthesis. Adv Mater. 2013;25:1813–21.
[48] Saldanha PL, Lesnyak V, Manna L. Large scale syntheses of colloidal nanomaterials. Nano Today. 2017;12:46–63.
[49] Maceiczyk RM, Lignos IG. Online detection and automation methods in microfluidic nanomaterial synthesis. Curr Opin Chem Eng. 2015;8:29–35.
[50] Park JI, Saffari A, Kumar S, Günther A, Kumacheva E. Microfluidic synthesis of polymer and inorganic particulate materials. Annu Rev Mater Res. 2010;40:415–43.
[51] Shestopalov I, Tice JD, Ismagilov RF. Multi-step synthesis of nanoparticles performed on millisecond time scale in a microfluidic droplet-based system. Lab Chip. 2004;4:316–21.
[52] Zhao C-X, He L, Qiao SZ, Middelberg APJ. Nanoparticle synthesis in microreactors. Chem Eng Sci. 2011;66:1463–79.
[53] Niu G, Ruditskiy A, Vara M, Xia Y. Toward continuous and scalable production of colloidal nanocrystals by switching from batch to droplet reactors. Chem Soc Rev. 2015;44:5806–20.
[54] Shang L, Cheng Y, Zhao Y. Emerging droplet microfluidics. Chem Rev. 2017;117:7964–8040.
[55] Pan LJ, Tu JW, Ma HT, Yang YJ, Tian ZQ, Pang DW, et al. Controllable synthesis of nanocrystals in droplet reactors. Lab Chip. 2018;18:41–56.
[56] Kim JH, Jeon TY, Choi TM, Shim TS, Kim S-H, Yang S-M. Droplet microfluidics for producing functional microparticles. Langmuir. 2013;30:1473–88.

[57] Alexandridis P. Gold nanoparticle synthesis, morphology control, and stabilization facilitated by functional polymers. Chem Eng Technol. 2011;34:15–28.
[58] Grzelczak M, Pérez-Juste J, Mulvaney P, Liz-Marzán LM. Shape control in gold nanoparticle synthesis. Chem Soc Rev. 2008;37:1783–91.
[59] Guo S, Wang E. Synthesis and electrochemical applications of gold nanoparticles. Anal Chim Acta. 2007;598:181–92.
[60] Zhao P, Li N, Astruc D. State of the art in gold nanoparticle synthesis. Coord Chem Rev. 2013;257:638–65.
[61] Günther A, Jensen KF. Multiphase microfluidics: from flow characteristics to chemical and materials synthesis. Lab Chip. 2006;6:1487–503.
[62] Song Y, Hormes J, Kumar CS. Microfluidic synthesis of nanomaterials. Small. 2008;4: 698–711.
[63] Shahbazali E, Hessel V, Noël T, Wang Q. Metallic nanoparticles made in flow and their catalytic applications in organic synthesis. Nanotechnol Rev. 2014;3:65–86.
[64] Sebastian V, Khan SA, Kulkarni AA. Flow synthesis of functional materials. J Flow Chem. 2017;7:96–105.
[65] Navin CV, Krishna KS, Theegala CS, Kumar CS. Lab-on-a-chip devices for gold nanoparticle synthesis and their role as a catalyst support for continuous flow catalysis. Nanotechnol Rev. 2014;3:39–63.
[66] Levenspiel O. Chemical reaction engineering, 3rd ed. Weinheim: John Wiley & Sons, 1999
[67] Wang ZL. Transmission electron microscopy of shape-controlled nanocrystals and their assemblies. J Phys Chem B. 2000;104:1153–75.
[68] Young NP, Van Huis MA, Zandbergen HW, Xu H, Kirkland AI. Transformations of gold nanoparticles investigated using variable temperature high-resolution transmission electron microscopy. Ultramicroscopy. 2010;110:506–16.
[69] Georgiev P, Bojinova A, Kostova B, Momekova D, Bjornholm T, Balashev K. Implementing atomic force microscopy (AFM) for studying kinetics of gold nanoparticle's growth. Colloids Surf. A. 2013;434:154–63.
[70] Khlebtsov BN, Khlebtsov NG. On the measurement of gold nanoparticle sizes by the dynamic light scattering method. Colloid J. 2011;73:118–27.
[71] Du Toit H, Macdonald T, Huang H, Parkin I, Gavriilidis A. Continuous flow synthesis of citrate capped gold nanoparticles using UV induced nucleation. RSC Adv. 2017;7:9632–38.
[72] Chaki NK, Negishi Y, Tsunoyama H, Shichibu Y. Ubiquitous 8 and 29 kDa gold: alkanethiolate cluster compounds: mass-spectrometric determination of molecular formulas and structural implications. J Am Chem Soc. 2008;130:8608–10.
[73] Kettemann F, Birnbaum A, Witte S, Wuithschick M, Pinna N, Kraehnert R, et al. Missing piece of the mechanism of the Turkevich method: the critical role of citrate protonation. Chem Mater. 2016;28:4072–81.
[74] Abécassis B, Testard F, Spalla O, Barboux P. Probing in situ the nucleation and growth of gold nanoparticles by small-angle X-ray scattering. Nano Lett. 2007;7:1723–27.
[75] Polte J, Erler R, Thünemann AF, Emmerling F, Kraehnert R. SAXS in combination with a free liquid jet for improved time-resolved in situ studies of the nucleation and growth of nanoparticles. Chem Commun. 2010;46:9209–11.
[76] Polte J, Erler R, ThüNemann AF, Sokolov S, Ahner TT, Rademann K, et al. Nucleation and growth of gold nanoparticles studied via in situ small angle X-ray scattering at millisecond time resolution. ACS Nano. 2010;4:1076–82.
[77] Abécassis B, Testard F, Kong Q, Francois B, Spalla O. Influence of monomer feeding on a fast gold nanoparticles synthesis: time-resolved XANES and SAXS experiments. Langmuir. 2010;26:13847–54.

[78] Polte J, Ahner TT, Delissen F, Sokolov S, Emmerling F, Thunemann AF, et al. Mechanism of gold nanoparticle formation in the classical citrate synthesis method derived from coupled in situ XANES and SAXS evaluation. J Am Chem Soc. 2010;132:1296–301.
[79] Kwon K, Lee KY, Lee YW, Kim M, Heo J, Ahn SJ, et al. Controlled synthesis of icosahedral gold nanoparticles and their surface-enhanced Raman scattering property. J Phys Chem C. 2007;111:1161–65.
[80] Allabashi R, Stach W, De La Escosura-Muñiz A, Liste-Calleja L, Merkoçi A. ICP-MS: a powerful technique for quantitative determination of gold nanoparticles without previous dissolving. J Nanopart Res. 2008;11:2003.
[81] Laborda F, Bolea E, Jiménez-Lamana J. Single particle inductively coupled plasma mass spectrometry: a powerful tool for nanoanalysis. Anal Chem. 2014;86:2270–8.
[82] Dequaire M, Degrand C, Limoges B. An electrochemical metalloimmunoassay based on a colloidal gold label. Anal Chem. 2000;72:5521–8.
[83] González García MB, Costa García A. Adsorptive stripping voltammetric behaviour of colloidal gold and immunogold on carbon paste electrode. Bioelectrochem Bioenerg. 1995;38:389–95.
[84] Pumera M, Aldavert M, Mills C, Merkoçi A, Alegret S. Direct voltammetric determination of gold nanoparticles using graphite-epoxy composite electrode. Electrochim Acta. 2005;50:3702–7.
[85] Welz B, Becker-Ross H, Florek S, Heitmann U. High-resolution continuum source AAS: the better way to do atomic absorption spectrometry. Weinheim: John Wiley & Sons, 2006
[86] Elzey S, Tsai DH, Rabb SA, Yu LL, Winchester MR, Hackley VA. Quantification of ligand packing density on gold nanoparticles using ICP-OES. Anal Bioanal Chem. 2012;403:145–9.
[87] Hendel T, Lesnyak V, Kühn L, Herrmann AK, Bigall NC, Borchardt L, et al. Mixed aerogels from Au and CdTe nanoparticles. Adv Funct Mater. 2013;23:1903–11.
[88] Liu X, Atwater M, Wang J, Huo Q. Extinction coefficient of gold nanoparticles with different sizes and different capping ligands. Colloids Surf. B. 2007;58:3–7.
[89] Kattumuri V, Katti K, Bhaskaran S, Boote EJ, Casteel SW, Fent GM, et al. Gum arabic as a phytochemical construct for the stabilization of gold nanoparticles: in vivo pharmacokinetics and X-ray-contrast-imaging studies. Small. 2007;3:333–41.
[90] Park J, Shumaker-Parry JS. Structural study of citrate layers on gold nanoparticles: role of intermolecular interactions in stabilizing nanoparticles. J Am Chem Soc. 2014;136:1907–21.
[91] Koziej D. Revealing complexity of nanoparticle synthesis in solution by in situ hard X-ray spectroscopy – today and beyond. Chem Mater. 2016;28:2478–90.
[92] Ohyama J, Teramura K, Higuchi Y, Shishido T, Hitomi Y, Aoki K, et al. An in situ quick XAFS spectroscopy study on the formation mechanism of small gold nanoparticles supported by porphyrin-cored tetradentate passivants. Phys Chem Chem Phys. 2011;13:11128–35.
[93] Zhang P, Sham T. X-ray studies of the structure and electronic behavior of alkanethiolate-capped gold nanoparticles: the interplay of size and surface effects. Phys Rev Lett. 2003;90:245502.
[94] Park J-W, Shumaker-Parry JS. Strong resistance of citrate anions on metal nanoparticles to desorption under thiol functionalization. ACS Nano. 2015;9:1665–82.
[95] Badia A, Cuccia L, Demers L, Morin F, Lennox RB. Structure and dynamics in alkanethiolate monolayers self-assembled on gold nanoparticles: a DSC, FT-IR, and deuterium NMR study. J Am Chem Soc. 1997;119:2682–92.
[96] Ji X, Song X, Li J, Bai Y, Yang W, Peng X. Size control of gold nanocrystals in citrate reduction: the third role of citrate. J Am Chem Soc. 2007;129:13939–48.
[97] Wuithschick M, Birnbaum A, Witte S, Sztucki M, Vainio U, Pinna N, et al. Turkevich in new robes: key questions answered for the most common gold nanoparticle synthesis. ACS Nano. 2015;9:7052–71.

[98] Boleininger J, Kurz A, Reuss V, Sönnichsen C. Microfluidic continuous flow synthesis of rod-shaped gold and silver nanocrystals. Phys Chem Chem Phys. 2006;8:3824–7.
[99] Pellegrino T, Sperling RA, Alivisatos AP, Parak WJ. Gel electrophoresis of gold-DNA nanoconjugates. Journal of Biomedicine and Biotechnology. 2007;2007:Article ID 26796.
[100] Haiss W, Thanh NTK, Aveyard J, Fernig DG. Determination of size and concentration of gold nanoparticles from UV–Vis spectra. Anal Chem. 2007;79:4215–21.
[101] Hendel T, Wuithschick M, Kettemann F, Birnbaum A, Rademann K, Polte J. In situ determination of colloidal gold concentrations with UV–Vis spectroscopy: limitations and perspectives. Anal Chem. 2014;86:11115–24.
[102] Liz-Marzán LM. Tailoring surface plasmons through the morphology and assembly of metal nanoparticles. Langmuir. 2006;22:32–41.
[103] Schneider G, Decher G. From functional core/shell nanoparticles prepared via layer-by-layer deposition to empty nanospheres. Nano Lett. 2004;1833–9.
[104] Peck JA, Tait CD, Swanson BI, Brown GE. Speciation of aqueous gold (III) chlorides from ultraviolet/visible absorption and Raman/resonance Raman spectroscopies. Geochim Cosmochim Acta. 1991;55:671–6.
[105] Becker R, Doring W. Kinetic treatment of the nucleation in supersaturated vapors. Washington: National Advisory Committee for Aeronautics, 1954
[106] LaMer VK, Dinegar RH. Theory, production and mechanism of formation of monodispersed hydrosols. J Am Chem Soc. 1950;72:4847–54.
[107] Bogush GH, Zukoski CF. IV, Uniform silica particle precipitation: an aggregative growth model. J Colloid Interface Sci. 1991;142:19–34.
[108] Watzky MA, Finke RG. Transition metal nanocluster formation kinetic and mechanistic studies. a new mechanism when hydrogen is the reductant: slow, continuous nucleation and fast autocatalytic surface growth. J Am Chem Soc. 1997;119:10382–400.
[109] Zeng XC, Oxtoby DW. Gas–Liquid nucleation in Lennard–Jones fluids. J Chem Phys. 1991;94:4472–8.
[110] Xia Y, Xiong Y, Lim B, Skrabalak SE. Shape-controlled synthesis of metal nanocrystals: simple chemistry meets complex physics? Angew Chem Int Ed. 2009;48:60–103.
[111] Polte J. Fundamental growth principles of colloidal metal nanoparticles – A new perspective. Cryst Eng Comm. 2015;17:6809–30.
[112] Luty-Blocho M, Pacławski K, Jaworski W, Streszewski B, Fitzner K. Kinetic studies of gold nanoparticles formation in the batch and in the flow microreactor system. Trends in colloid and interface science XXIV, Progr Colloid Polym Sci Vol. 138. Berlin: Springer, 2011:39–44.
[113] Pacławski K, Streszewski B, Jaworski W, Luty-Błocho M, Fitzner K. Gold nanoparticles formation via gold (III) chloride complex ions reduction with glucose in the batch and in the flow microreactor systems. Colloids Surf. A. 2012;413:208–15.
[114] De Jonge N, Ross FM. Electron microscopy of specimens in liquid. Nat Nanotechnol. 2011;6:695–704.
[115] Kim BH, Yang J, Lee D, Choi BK, Hyeon T, Park J. Liquid-phase transmission electron microscopy for studying colloidal inorganic nanoparticles. Adv Mater. 2018;30:1–20.
[116] Baumgartner J, Dey A, Bomans PHH, Le Coadou C, Fratzl P, Sommerdijk NAJM, et al. Nucleation and growth of magnetite from solution. Nat Mater. 2013;12:310–14.
[117] McKenzie LC, Haben PM, Kevan SD, Hutchison JE. Determining nanoparticle size in real time by small-angle X-ray scattering in a microscale flow system. J Phys Chem C. 2010;114:22055–63.
[118] Watt J, Hance BG, Anderson RS, Huber DL. Effect of seed age on gold nanorod formation: a microfluidic, real-time investigation. Chem Mater. 2015;27:6442–9.
[119] Buining PA, Humbel BM, Philipse AP, Verkleij AJ. Preparation of functional silane-stabilized gold colloids in the (sub) nanometer size range. Langmuir. 1997;13:3921–6.

[120] Tofighi G, Lichtenberg H, Pesek J, Sheppard TL, Wang W, Schöttner L, et al. Continuous microfluidic synthesis of colloidal ultrasmall gold nanoparticles: in situ study of the early reaction stages and application for catalysis. React Chem Eng. 2017;2:876–84.
[121] Yue J, Falke FH, Schouten JC, Nijhuis TA. Microreactors with integrated UV/Vis spectroscopic detection for online process analysis under segmented flow. Lab Chip. 2013;13:4855–63.
[122] Sai Krishna K, Navin CV, Biswas S, Singh V, Ham K, Bovenkamp GL, et al. Millifluidics for time-resolved mapping of the growth of gold nanostructures. J Am Chem Soc. 2013;135:5450–6.
[123] Barnard AS. Modelling of nanoparticles: approaches to morphology and evolution. Rep Prog Phys. 2010;73:086502.
[124] Ojea-Jiménez I, Campanera JM. Molecular modeling of the reduction mechanism in the citrate-mediated synthesis of gold nanoparticles. J Phys Chem C. 2012;116:23682–91.
[125] Grochola G, Snook IK, Russo SP. Computational modeling of nanorod growth. J Chem Phys. 2007;127:194707.
[126] Häkkinen H. The gold–Sulfur interface at the nanoscale. Nat Chem. 2012;4:443.
[127] Taylor MG, Mpourmpakis G. Thermodynamic stability of ligand-protected metal nanoclusters. Nat Commun. 2017;8:15988.
[128] Ramkrishna D. Population balances – theory and applications to particulate systems in engineering, 1. Academic Press, 2000:355.
[129] Crowley T. Control of particle size distribution described by a population balance model of semibatch emulsion polymerization. J Process Control. 2000;10:419–32.
[130] Immanuel CD, Doyle FJ, III. Computationally efficient solution of population balance models incorporating nucleation, growth and coagulation: application to emulsion polymerization. Chem Eng Sci. 2003;58:3681–98.
[131] Kotoulas C, Kiparissides C. A generalized population balance model for the prediction of particle size distribution in suspension polymerization reactors. Chem Eng Sci. 2006;61:332–46.
[132] Marchal P, David R, Klein JP, Villermaux J. Crystallization and precipitation engineering-I. An efficient method for solving population balance in crystallization with agglomeration. Chem Eng Sci. 1988;43:59–67.
[133] Puel F, Févotte G, Klein JP. Simulation and analysis of industrial crystallization processes through multidimensional population balance equations. Part 1: a resolution algorithm based on the method of classes. Chem Eng Sci. 2003;58:3715–27.
[134] Puel F, Févotte G, Klein JP. Simulation and analysis of industrial crystallization processes through multidimensional population balance equations. Part 2: a study of semi-batch crystallization. Chem Eng Sci. 2003;58:3729–40.
[135] Bogush GH, Zukoski CF, IV. Studies of the kinetics of the precipitation of uniform silica particles through the hydrolysis and condensation of silicon alkoxides. J Colloid Interface Sci. 1991;142:1–18.
[136] Park J, Joo J, Soon GK, Jang Y, Hyeon T. Synthesis of monodisperse spherical nanocrystals. Angew Chem Int Ed. 2007;46:4630–60.
[137] Stolzenburg P, Garnweitner G. Experimental and numerical insights into the formation of zirconia nanoparticles: a population balance model for the nonaqueous synthesis. React Chem Eng. 2017;2:337–48.
[138] Rempel JY, Bawendi MG, Jensen KF. Insights into the kinetics of semiconductor nanocrystal nucleation and growth. J Am Chem Soc. 2009;131:4479–89.
[139] Maceiczyk RM, Bezinge L, deMello AJ. Kinetics of nanocrystal synthesis in a microfluidic reactor: theory and experiment. React Chem Eng. 2016;1:261–71.
[140] Lazzari S, Abolhasani M, Jensen KF. Modeling of the formation kinetics and size distribution evolution of II–VI quantum dots. React Chem Eng. 2017;2:567–76.

[141] Perala SRK, Kumar S. On the mechanism of metal nanoparticle synthesis in the Brust-Schiffrin method. Langmuir. 2013;29:9863–73.
[142] Kumar S, Gandhi K, Kumar R. Modeling of formation of gold nanoparticles by citrate method. Ind Eng Chem Res. 2007;46:3128–36.
[143] Agunloye E, Gavriilidis A, Mazzei L. A mathematical investigation of the Turkevich organizer theory in the citrate method for the synthesis of gold nanoparticles. Chem Eng Sci. 2017;173:275–86.
[144] Turkevich J, Stevenson PC, Hillier J. A study of the nucleation and growth processes in the synthesis of colloidal gold. Discuss Faraday Soc. 1951;11:55–75.
[145] Biggs S, Chow M, Zukoski CF, Grieser F. The role of colloidal stability in the formation of gold sols. J Colloid Interface Sci. 1993;160:511–13.
[146] Frens G. Controlled nucleation for the regulation of the particle size in monodisperse gold suspensions. Nature. 1973;241:20–2.
[147] Kimling J, Maier M, Okenve B, Kotaidis V, Ballot H, Plech A. Turkevich method for gold nanoparticle synthesis revisited. J Phys Chem B. 2006;110:15700–7.
[148] Sivaraman SK, Kumar S, Santhanam V. Monodisperse sub-10 nm gold nanoparticles by reversing the order of addition in Turkevich method–The role of chloroauric acid. J Colloid Interface Sci. 2011;361:543–47.
[149] Xia H, Bai S, Hartmann JR, Wang D. Synthesis of monodisperse quasi-spherical gold nanoparticles in water via silver (I)-assisted citrate reduction. Langmuir. 2009;26:3585–9.
[150] Schulz F, Homolka T, Bastús NG, Puntes V, Weller H, Vossmeyer T. Little adjustments significantly improve the Turkevich synthesis of gold nanoparticles. Langmuir. 2014;30:10779–84.
[151] Bastús NG, Comenge J, Puntes V. Kinetically controlled seeded growth synthesis of citrate-stabilized gold nanoparticles of up to 200 nm: size focusing versus Ostwald ripening. Langmuir. 2011;27:11098–105.
[152] Ziegler C, EychmüLler A. Seeded growth synthesis of uniform gold nanoparticles with diameters of 15–300 nm. J Phys Chem C. 2011;115:4502–06.
[153] Piella J, Bastús NG, Puntes V. Size-controlled synthesis of sub-10-nanometer citrate-stabilized gold nanoparticles and related optical properties. Chem Mater. 2016;28:1066–75.
[154] Slot JW, Geuze HJ. A new method of preparing gold probes for multiple-labeling cytochemistry. Eur J Cell Biol. 1985;38:87–93.
[155] Brown KR, Fox AP, Natan MJ. Morphology-dependent electrochemistry of cytochrome c at Au colloid-modified SnO_2 electrodes. J Am Chem Soc. 1996;118:1154–7.
[156] Singh A, Shirolkar M, Lalla NP, Malek CK, Kulkarni S. Room temperature, water-based, microreactor synthesis of gold and silver nanoparticles. Int J Nanotechnol. 2009;6:541–51.
[157] Brust M, Walker M, Bethell D, Schiffrin DJ, Whyman R. Synthesis of thiol-derivatised gold nanoparticles in a two-phase liquid–liquid system. J Chem Soc, Chem Commun. 1994;0:801–2
[158] Jun H, Fabienne T, Florent M, Coulon P-E, Nicolas M, Olivier S. Understanding of the size control of biocompatible gold nanoparticles in millifluidic channels. Langmuir. 2012;28:15966–74.
[159] Shalom D, Wootton RC, Winkle RF, Cottam BF, Vilar R, Wilde CP. Synthesis of thiol functionalized gold nanoparticles using a continuous flow microfluidic reactor. Mater Lett. 2007;61:1146–50.
[160] Tsunoyama H, Ichikuni N, Tsukuda T. Microfluidic synthesis and catalytic application of PVP-stabilized, ~1 nm gold clusters. Langmuir. 2008;24:11327–30.
[161] Luty-Błocho M, Fitzner K, Hessel V, Löb P, Maskos M, Metzke D, et al. Synthesis of gold nanoparticles in an interdigital micromixer using ascorbic acid and sodium borohydride as reducers. Chem Eng J. 2011;171:279–90.
[162] Köhler J, Wagner J, Albert J. Formation of isolated and clustered Au nanoparticles in the presence of polyelectrolyte molecules using a flow-through Si chip reactor. J Mater Chem. 2005;15:1924–30.
[163] Wagner J, Köhler JM. Continuous synthesis of gold nanoparticles in a microreactor. Nano Lett. 2005;5:685–91.

[164] Wagner J, Tshikhudo TR, Köhler JM. Microfluidic generation of metal nanoparticles by borohydride reduction. Chem Eng J. 2007;135:104–9.
[165] Sugano K, Uchida Y, Ichihashi O, Yamada H, Tsuchiya T, Tabata O. Mixing speed-controlled gold nanoparticle synthesis with pulsed mixing microfluidic system. Microfluid Nanofluidics. 2010;9:1165–74.
[166] Verma M, Kumaran V. Effect of ultra-fast mixing in a microchannel due to a soft wall on the room temperature synthesis of gold nanoparticles. Sadhana. 2015;40:973–83.
[167] Bandulasena MV, Vladisavljević GT, Odunmbaku OG, Benyahia B. Continuous synthesis of PVP stabilized biocompatible gold nanoparticles with a controlled size using a 3D glass capillary microfluidic device. Chem Eng Sci. 2017;171:233–43.
[168] Baber R, Mazzei L, Thanh NTK, Gavriilidis A. An engineering approach to synthesis of gold and silver nanoparticles by controlling hydrodynamics and mixing based on a coaxial flow reactor. Nanoscale. 2017;9:14149–61.
[169] Yang SY, Cheng FY, Yeh CS, Lee GB. Size-controlled synthesis of gold nanoparticles using a micro-mixing system. Microfluid Nanofluidics. 2009;8:303–11.
[170] Kitson PJ, Rosnes MH, Sans V, Dragone V, Cronin L. Configurable 3D-printed millifluidic and microfluidic 'lab on a chip' reactionware devices. Lab Chip. 2012;12:3267–71.
[171] Ftouni J, Penhoat M, Addad A, Payen E, Rolando C, Girardon J-S. Highly controlled synthesis of nanometric gold particles by citrate reduction using the short mixing, heating and quenching times achievable in a microfluidic device. Nanoscale. 2012;4:4450–4.
[172] Jamal F, Jean-Sébastien G, Maël P, Edmond P, Christian R. Gold nanoparticle synthesis in microfluidic systems and immobilisation in microreactors designed for the catalysis of fine organic reactions. MicrosystTechnol. 2012;18:151–58.
[173] Gómez-De Pedro S, Puyol M, Alonso-Chamarro J. Continuous flow synthesis of nanoparticles using ceramic microfluidic devices. Nanotechnology. 2010;21:415603.
[174] Sugie A, Song H, Horie T, Ohmura N, Kanie K, Muramatsu A, et al. Synthesis of thiol-capped gold nanoparticle with a flow system using organosilane as a reducing agent. Tetrahedron Lett. 2012;53:4457–59.
[175] Kumar DR, Kulkarni A, Prasad B. Microfluidic platform for continuous flow synthesis of triangular gold nanoplates. Colloids Surf., A. 2014;443:149–55.
[176] Fu Q, Ran G, Xu W. A microfluidic-based controllable synthesis of rolled or rigid ultrathin gold nanoplates. RSC Adv. 2015;5:37512–6.
[177] Sebastián V, Lee S, Zhou C, Kraus MF, Fujimoto JG, Jensen KF. One-step continuous synthesis of biocompatible gold nanorods for optical coherence tomography. Chem Commun. 2012;48:6654–6.
[178] Ishizaka T, Ishigaki A, Kawanami H, Suzuki A, Suzuki TM. Dynamic control of gold nanoparticle morphology in a microchannel flow reactor by glucose reduction in aqueous sodium hydroxide solution. J Colloid Interface Sci. 2012;367:135–8.
[179] Wagner J, Kirner T, Mayer G, Albert J, Köhler J. Generation of metal nanoparticles in a microchannel reactor. Chem Eng J. 2004;101:251–60.
[180] Sebastian V, Khan SA, Kulkarni AA. Perspective article: flow synthesis of functional materials. J Flow Chem. 2017;7:96–105.
[181] Lohse SE, Eller JR, Sivapalan ST, Plews MR, Murphy CJ. A simple millifluidic benchtop reactor system for the high-throughput synthesis and functionalization of gold nanoparticles with different sizes and shapes. ACS Nano. 2013;7:4135–50.
[182] Gomez L, Sebastian V, Irusta S, Ibarra A, Arruebo M, Santamaria J. Scaled-up production of plasmonic nanoparticles using microfluidics: from metal precursors to functionalized and sterilized nanoparticles. Lab Chip. 2014;14:325–32.
[183] Uson L, Sebastian V, Arruebo M, Santamaria J. Continuous microfluidic synthesis and functionalization of gold nanorods. Chem Eng J. 2016;285:286–92.

[184] Bullen C, Latter MJ, D'Alonzo NJ, Willis GJ, Raston CL. A seedless approach to continuous flow synthesis of gold nanorods. Chem Commun. 2011;47:4123–5.
[185] Sans V, Glatzel S, Douglas FJ, Maclaren DA, Lapkin A, Cronin L. Non-equilibrium dynamic control of gold nanoparticle and hyper-branched nanogold assemblies. Chem Sci. 2014;5:1153–7.
[186] Bayazit MK, Yue J, Cao E, Gavriilidis A, Tang J. Controllable synthesis of gold nanoparticles in aqueous solution by microwave assisted flow chemistry. ACS Sustain Chem Eng. 2016;4:6435–42.
[187] Köhler JM, Li S, Knauer A. Why is micro segmented flow particularly promising for the synthesis of nanomaterials? Chem Eng Technol. 2013;36:887–99.
[188] Liu H, Vandu CO, Krishna R. Hydrodynamics of Taylor flow in vertical capillaries: flow regimes, bubble rise velocity, liquid slug length, and pressure drop. Ind Eng Chem Res. 2005;44:4884–97.
[189] Sebastian Cabeza V, Kuhn S, Kulkarni AA, Jensen KF. Size-controlled flow synthesis of gold nanoparticles using a segmented flow microfluidic platform. Langmuir. 2012;28:7007–13.
[190] Kulkarni AA, Sebastian Cabeza V. Insights in the diffusion controlled interfacial flow synthesis of Au nanostructures in a microfluidic system. Langmuir. 2017;33:14315–24.
[191] In: Ngai T, Bon SAF, editor(s). Particle-stabilized emulsions and colloids. Cambridge: Royal Society of Chemistry, 2014
[192] Khan SA, Duraiswamy S. Controlling bubbles using bubbles – microfluidic synthesis of ultra-small gold nanocrystals with gas-evolving reducing agents. Lab Chip. 2012;12:1807–12.
[193] Song H, Tice JD, Ismagilov RF. A microfluidic system for controlling reaction networks in time. Angew Chem. 2003;115:792–6.
[194] Günther A, Jhunjhunwala M, Thalmann M, Schmidt MA, Jensen KF. Micromixing of miscible liquids in segmented gas–liquid flow. Langmuir. 2005;21:1547–55.
[195] Zhang L, Xia Y. Scaling up the production of colloidal nanocrystals: should we increase or decrease the reaction volume? Adv Mater. 2014;26:2600–6.
[196] Christopher GF, Anna SL. Microfluidic methods for generating continuous droplet streams. J Phys D Appl Phys. 2007;40:R319.
[197] Garstecki P, Fuerstman MJ, Stone HA, Whitesides GM. Formation of droplets and bubbles in a microfluidic T-junction – scaling and mechanism of break-up. Lab Chip. 2006;6:437–46.
[198] Duraiswamy S, Khan SA. Droplet-based microfluidic synthesis of anisotropic metal nanocrystals. Small. 2009;5:2828–34.
[199] Duraiswamy S, Khan SA. Dual-stage continuous-flow seedless microfluidic synthesis of anisotropic gold nanocrystals. Part Part Syst Charact. 2014;31:429–32.
[200] Duraiswamy S, Khan SA. Plasmonic nanoshell synthesis in microfluidic composite foams. Nano Lett. 2010;10:3757–63.
[201] Lazarus LL, Yang AS, Chu S, Brutchey RL, Malmstadt N. Flow-focused synthesis of monodisperse gold nanoparticles using ionic liquids on a microfluidic platform. Lab Chip. 2010;10:3377–9.
[202] Lazarus LL, Riche CT, Marin BC, Gupta M, Malmstadt N, Brutchey RL. Two-phase microfluidic droplet flows of ionic liquids for the synthesis of gold and silver nanoparticles. ACS Appl Mater Interfaces. 2012;4:3077–83.
[203] Taifur-Rahman M, Krishnamurthy PG, Parthiban P, Jain A, Park CP, Kim D-P, et al. Dynamically tunable nanoparticle engineering enabled by short contact-time microfluidic synthesis with a reactive gas. RSC Adv. 2013;3:2897–900.
[204] Abalde-Cela S, Taladriz-Blanco P, De Oliveira MG, Abell C. Droplet microfluidics for the highly controlled synthesis of branched gold nanoparticles. Sci Rep. 2018;8:2440.
[205] Hafermann L, Köhler JM. Small gold nanoparticles formed by rapid photochemical flow-through synthesis using microfluid segment technique. J Nanopart Res. 2015;17:1–8.
[206] Lee KG, Hong J, Wang KW, Heo NS, Kim DH, Lee SY, et al. In vitro biosynthesis of metal nanoparticles in microdroplets. ACS Nano. 2012;6:6998–7008.

[207] Gu T, Zheng C, He F, Zhang Y, Khan SA, Hatton TA. Electrically controlled mass transport into microfluidic droplets from nanodroplet carriers with application in controlled nanoparticle flow synthesis. Lab Chip. 2018;18:1330–40.
[208] Zhang L, Niu G, Lu N, Wang J, Tong L, Wang L, et al. Continuous and scalable production of well-controlled noble-metal nanocrystals in milliliter-sized droplet reactors. Nano Lett. 2014;14:6626–31.
[209] Yang Y, Serrano González LA, Guldin S. A versatile AuNP synthetic platform for decoupled control of size and surface composition. Langmuir. 2018;34:6820–6
[210] Rossi D, Gargiulo L, Valitov G, Gavriilidis A, Mazzei L. Experimental characterization of axial dispersion in coiled flow inverters. Chem Eng Res Des. 2017;120:159–70.
[211] Trachsel F, Günther A, Khan S, Jensen KF. Measurement of residence time distribution in microfluidic systems. Chem Eng Sci. 2005;60:5729–37.
[212] Günther A, Khan SA, Thalmann M, Trachsel F, Jensen KF. Transport and reaction in microscale segmented gas-liquid flow. Lab Chip. 2004;4:278–86.
[213] Khan SA, Günther A, Schmidt MA, Jensen KF. Microfluidic synthesis of colloidal silica. Langmuir. 2004;20:8604–11.
[214] Krishnadasan S, Tovilla J, Vilar R, deMello AJ, deMello JC. On-line analysis of CdSe nanoparticle formation in a continuous flow chip-based microreactor. J Mater Chem. 2004;14:2655.
[215] Panariello L, Mazzei L, Gavriilidis A. Modelling the synthesis of nanoparticles in continuous microreactors: the role of diffusion and residence time distribution on nanoparticle characteristics. Chem Eng J. 2018;350:1144–54
[216] Marchisio DL, Rivautella L, Barresi AA. Design and scale-up of chemical reactors for nanoparticle precipitation. AIChE J. 2006; 1877–87.
[217] Tae G, Lammertink RG, Kornfield JA, Hubbell JA. Facile hydrophilic surface modification of poly (tetrafluoroethylene) using fluoroalkyl-terminated poly(ethylene glycol)s. Adv Mater. 2003;15:66–9.
[218] Zhang L, Wang Y, Tong L, Xia Y. Synthesis of colloidal metal nanocrystals in droplet reactors: the pros and cons of interfacial adsorption. Nano Lett. 2014;14:4189–94.
[219] Weeranoppanant N, Adamo A, Saparbaiuly G, Rose E, Fleury C, Schenkel B, et al. Design of multistage counter-current liquid–Liquid extraction for small-scale applications. Ind Eng Chem Res. 2017;56:4095–103.
[220] Sweeney SF, Woehrle GH, Hutchison JE. Rapid purification and size separation of gold nanoparticles via diafiltration. J Am Chem Soc. 2006;128:3190–97.

Bionotes

He Huang received her BS degree from the department of Chemical Engineering, Dalian University of Technology (Liaoning Province, China) in 2012. She obtained an MSc degree in 2014 and continued her study as a PhD candidate at the department of Chemical Engineering, University College London under the supervision of Prof. Gavriilidis. Her research area is the controlled synthesis of gold nanocrystals in microfluidic systems.

Hendrik du Toit received an MEng in Chemical Engineering from Imperial College London in 2011. He subsequently received his PhD from the University of Bath in 2015 whilst conducting research into the production of biocompatible biosensors and biofuel cells for implantable medical devices. He then joined Prof. Gavriilidis' research group at University College London where his focus has been on developing continuous flow gold nanoparticle synthesis systems. His research interests include fuel cells, biosensing, nanomaterials, fluidic technologies and reactor design.

Luca Panariello received both a BS (2014) and MSc (2016) degree in Chemical Engineering with honours at the University of Naples "Federico II" (Italy). He joined the department of Chemical Engineering at University College London in 2016 in a joint research project with the University of Naples "Federico II". He was then awarded a Marie Skłodowska-Curie PhD scholarship in 2017 to work on process intensification of nanomaterials production under the supervision of Prof. Gavriilidis.

Luca Mazzei graduated in Chemical Engineering from the University of Naples "Federico II" (Italy) in 2001. He spent 3 years working for Technip KTI as a process and start-up engineer on sulphur recovery and refinery tail gas treatment. Subsequently he joined the Department of Chemical Engineering at University College London, first as a student, where he was awarded a PhD in 2008, and then promoted to Lecturer in 2009. His research activities deal with experimental and modelling of polydisperse multiphase systems, with focus on crystallization processes and nanoparticles synthesis, relying on advanced mathematical modelling and CFD.

Asterios Gavriilidis obtained a Diploma from the University of Thessaloniki (Greece) in 1988, and an MSc in 1990 and PhD in 1993 from the University of Notre Dame, USA, all in Chemical Engineering. He joined the Department of Chemical Engineering at University College London (UK) in 1993, where he has been professor of Chemical Reaction Engineering since 2004. His research interests include chemical and catalytic reaction engineering, microreaction and microprocess technology, continuous nanomaterials synthesis.